

Geometrically exact static isogeometric analysis of an arbitrarily curved spatial Bernoulli-Euler beam

A. Borković^{1,2}, B. Marussig¹, and G. Radenković^{2,3}

¹*Institute of Applied Mechanics, Graz University of Technology, Technikerstraße 4/II, 8010 Graz, Austria, aleksandar.borkovic@aggf.unibl.org, aborkovic@tugraz.at*

²*University of Banja Luka, Faculty of Architecture, Civil Engineering and Geodesy, Department of Mechanics and Theory of Structures, 78000 Banja Luka, Bosnia and Herzegovina*

³*Faculty of Civil Engineering, University of Belgrade, Bulevar kralja Aleksandra 73, 11000 Belgrade, Serbia*

Abstract

The objective of this research is the development of a geometrically exact model for the analysis of arbitrarily curved spatial Bernoulli-Euler beams. The complete metric of the beam is utilized in order to include the effect of curviness on the nonlinear distribution of axial strain over the cross section. The exact constitutive relation between energetically conjugated pairs is employed, along with four reduced relations. The isogeometric approach, which allows smooth connections between finite elements, is used for the spatial discretization of the weak form. Two methods for updating the local basis are applied and discussed in the context of finite rotations. All the requirements of geometrically exact beam theory are satisfied, such as objectivity and path-independence. The accuracy of the formulation is verified by a thorough numerical analysis. The influence of the curviness on the structural response is scrutinized for two classic examples. If the exact response of the structure is sought, the curviness must be considered when choosing the appropriate beam model.

Keywords: spatial Bernoulli-Euler beam; strongly curved beams; geometrically exact analysis; analytical constitutive relation;

1 Introduction

Contemporary engineering is facing a growing demand for novel types of cost-effective structures which are simultaneously resistant and flexible. This trend is encouraged by the development of new structural materials, the constant improvement of existing ones, and novel discoveries related to structural form-finding. Curved spatial beams are crucial components of these structures and their application is fundamental in various fields of engineering, molecular physics, electronics, bio-mechanics, optics, etc. In order to apply beam models to these new challenges, more accurate mathematical and mechanical models will be required.

First beam theories originate from the works of Euler and Bernoulli, later generalized by Kirchhoff, Clebsch, and Love [1]. There is great nomenclature diversity for beam theories and a study that makes a careful attempt to classify these is given in [2]. Accordingly, the subject of the presented research is an arbitrarily curved and twisted beam with an anisotropic solid cross section, without warping. If the assumption of rigid cross sections is applied, Simo-Reissner (SR) theory is obtained. The addition of the constraint that the cross section remains perpendicular to the deformed axis results with the Bernoulli-Euler (BE) theory.

The nonlinear theory of shear deformable curved spatial beams is proposed by Reissner [3]. Simo completed his work and introduced the term *geometrically exact beam theory* which comprises a formulation for which *the relationships between the configuration and the strain measures are consistent with the virtual work principle and the equilibrium equations at a deformed state regardless of the magnitude of displacements, rotations, and strains* [4]. This is often falsely referred to as a large strain theory despite the small strain assumption being present. Due to the presence of finite rotations, the configuration space of the GE beam theory is a special orthogonal (Lie) group, $SO(3)$. It is a nonlinear, differentiable manifold, whose associated group elements are not additive or commutative, which lead to various types of algorithms, [5, 6, 7, 8, 9, 10]. Recapitulation of these findings until 1997 is given in [11].

It is argued in [12, 13] that all finite element (FE) implementations of the geometrically exact beam theory, existent at that time, are non-objective and path-dependent. An orthogonal interpolation scheme that is independent of the vector parameterization of a rotation manifold is suggested. This paved the way for the development of many alternative rotation interpolation strategies, [14, 15, 16]. The corotational formulation employed in [17] and [18] preserves objectivity by definition. Recently, an improvement to the corotational approach for shear deformable beams is given in [19]. The carefully calculated corotational nodal rotations are interpolated which led to the satisfaction of all the requirements of the geometrically exact beam theory. The fact that many formulations do not deal with truly geometrically exact curved/twisted beams is discussed in [20].

The nonlinear analysis of spatial BE beams recently came under a similar focus of researchers. The problem of the invariance of classic curved beam theories is thoroughly elaborated in [21] and [22]. Membrane locking is another problem of thin curved BE beam which is treated by various techniques such as assumed strain or stress fields and reduced/selective integration [21]. Works [23] and [24] stand out due to their consistency with the geometrically exact approach. The most systematic up-to-date approach is the formulation by Meier et al. [25]. It satisfies many properties required by the geometrically exact analysis of a curved spatial slender BE beam. The effect of membrane locking is discussed in [26] while the beam-to-beam contact problem using a torsion-free beam model is considered in [27]. A comprehensive review of beam theories is given by the same authors in [2].

The isogeometric technique for the spatial discretization has attracted much attention [28]. The nonlinear shear-deformable spatial beam is readily considered in the framework of isogeometric analysis (IGA) [29, 30, 31, 32, 33, 34, 35]. Regarding the nonlinear analysis of BE beams in the context of IGA, a torsion- and rotation-free spatial cable formulation is developed in [36] with attractive nonlinear dynamic applications. A spatial BE beam modeled as a ribbon with four degrees of freedom (DOF) is introduced in [37] and extended

to the assemblies of beams in [38]. A mixed approach is considered in [39] while the consistent tangent operator is derived in [40]. Based on [37], the authors in [41] successfully performed nonlinear applications of a spatial curved BE beam. Recently, a multi-patch approach for the nonlinear analysis of BE beams is suggested [42]. The smallest rotation algorithm is used for an update of the basis. The nonlinear transformation between total cross-sectional rotations and unknown kinematics is defined in order to connect beams. An invariant geometric stiffness matrix is derived in [43] considering various end moments. However, the formulation is applied solely to the buckling analysis. The effect of initial curviness on the convergence properties of the solution procedure is considered in [44].

These works represent the state of the art of curved spatial BE beam theories. In contrast to the presented research, most of the reviewed literature disregards the higher order terms with respect to the beam cross-sectional metric. The majority of them also do not consider truly geometric exact nonlinear analysis due to their lack of objectivity. Recently, Radenković and Borković contributed to the linear static analysis of arbitrarily curved BE beams [45, 46], based on foundations given in [47]. The aim of this paper is to extend the developed formulation, which is applicable to strongly curved beams, to the nonlinear setting of geometrically exact beam theory.

For curved beams, axial and bending actions are coupled due to the nonlinear distribution of strain along the cross section. This distribution depends on *the curviness of beam* Kd . Here, K is the curvature of beam axis and d is the maximum dimension of the cross section in the planes parallel to the osculating plane [45]. Therefore, the term *arbitrarily curved beam* actually refers to a beam with arbitrary curviness. With respect to this parameter, curved beams are readily classified as small-, medium- or big-curvature beams [48]. We are here mostly concerned here with big-curvature, also known as *strongly curved*, beams, for which $Kd > 0.1$.

Although known for a long time, it is only recently that the strongly curved beams have been scrutinized in the framework of the modern numerical methods. Linear analysis of strongly curved plane beams is given in [49, 50, 51], while nonlinear analysis is considered in [52]. The linear response of spatial beams is analyzed in [45]. Here, we will consider the nonlinear behavior of prismatic BE beams of which some are strongly curved, i.e., $Kd > 0.1$, either locally or globally. To the best of our knowledge, this is the first paper that deals with the geometrically exact analysis of strongly curved spatial BE beams within the framework of IGA. The paper is based on our previous works [50, 51, 45, 47]. Its main contribution is the extension of the foundations given in [47, 45] to the geometrically exact setting by defining the appropriate basis update and the consistent derivation of the stiffness matrix. The geometric stiffness is found by the careful variation of both the internal and the external virtual power with respect to the unknown metric. Special care is devoted to the variation of the twist variable and its gradient. The exact geometry of the spatial BE beam is utilized for the derivation of weak form of equilibrium which is solved by the Newton-Raphson and arc-length methods. A strict derivation of the constitutive relation allows us to derive reduced models and to assess the effects of these simplifications through the numerical analysis. Comparison with existing results confirms that the obtained formulation is reliable for the finite rotation analysis of arbitrarily curved beams. Moreover, the approach introduces an additional level of accuracy when dealing with strongly curved beams. The present formulation is geometrically exact in a sense that it strictly defines a relation between work conjugate pairs which allows analysis of arbitrarily large rotations and displacements [4]. Furthermore, by the

careful implementation of the procedure for the basis update, the formulation is objective and path-independent [25].

The paper is structured as follows. The next section presents the basic relations of the beam metric and this is followed by the description of the BE beam kinematics. The finite element formulation is given in Section 4 and numerical examples are presented in Section 5. The conclusions are presented in the last section.

2 Metric of the beam continuum in the reference configuration

The metric of a spatial beam model at some reference configuration, is elaborated. The position of the beam axis and the orientation of the cross sections are thus required. The definition of the position of a spatial curve is trivial, while the orientation of the cross sections can be defined in several ways. One approach is to define the orientation of the cross section at the beginning of the beam, and to choose an operator of some kind to describe its relative orientation along the beam [37]. An alternative approach is to define a reference basis at each point of the beam axis, and then to define the material basis with respect to the reference one [25]. The latter approach is applied here by using the Frennet-Serret frame as the reference frame [45]. This frame represents the intrinsic frame of the beam axis since one of its basis vectors, \mathbf{n} , is aligned with the curvature vector of the beam axis, $\mathbf{c} = K\mathbf{n}$.

Boldface lowercase and uppercase letters are used for vectors and tensors/matrices, respectively. An asterisk sign is used to designate deformed configurations. Greek index letters take values of 2 and 3, while Latin ones take values of 1, 2 and 3. Partial and covariant derivatives with respect to the convective coordinates are designated with $(\bullet)_{,m}$ and $(\bullet)_{|m}$, respectively. Material time derivative is marked as $(\dot{\bullet})$.

For the details on the NURBS-based IGA modeling of curves, references [28, 53] are recommended.

2.1 Metric of the beam axis

A beam axis is defined by its position vector $\mathbf{r} = \mathbf{r}(\xi) = \mathbf{r}(s)$, with s being the arc-length coordinate while ξ is some arbitrary parametric coordinate Fig. 1. In general, setting up an arc-length parametrization of arbitrary curve is not possible in terms of elementary functions, hence ξ is usually employed for the parametrization of the beam axis.

The position vector of the beam axis is given in global Cartesian coordinates by:

$$\mathbf{r} = \mathbf{r}(\xi) = x^m(\xi)\mathbf{i}_m = x^m\mathbf{i}_m, \quad (x^1 = x, x^2 = y, x^3 = z). \quad (1)$$

Note that for the Cartesian coordinates, covariant and contravariant components are the same, and the position of indices is irrelevant. For every C^1 continuous curve, we can define a tangent vector:

$$\mathbf{g}_1 = \mathbf{r}_{,1} = \frac{d\mathbf{r}}{d\xi} = x^m_{,1}\mathbf{i}_m = \frac{d\mathbf{r}}{ds} \frac{ds}{d\xi} = \frac{ds}{d\xi} \mathbf{t}. \quad (2)$$

\mathbf{g}_1 is the tangent vector of an arbitrary length, while \mathbf{t} is the unit-length tangent of the beam axis. A function that defines the length of the basis vector \mathbf{g}_1 is:

$$\|\mathbf{g}_1\| = \sqrt{\mathbf{g}_1 \cdot \mathbf{g}_1} = \sqrt{g_{11}} = \sqrt{g} \implies ds = \sqrt{g} d\xi. \quad (3)$$

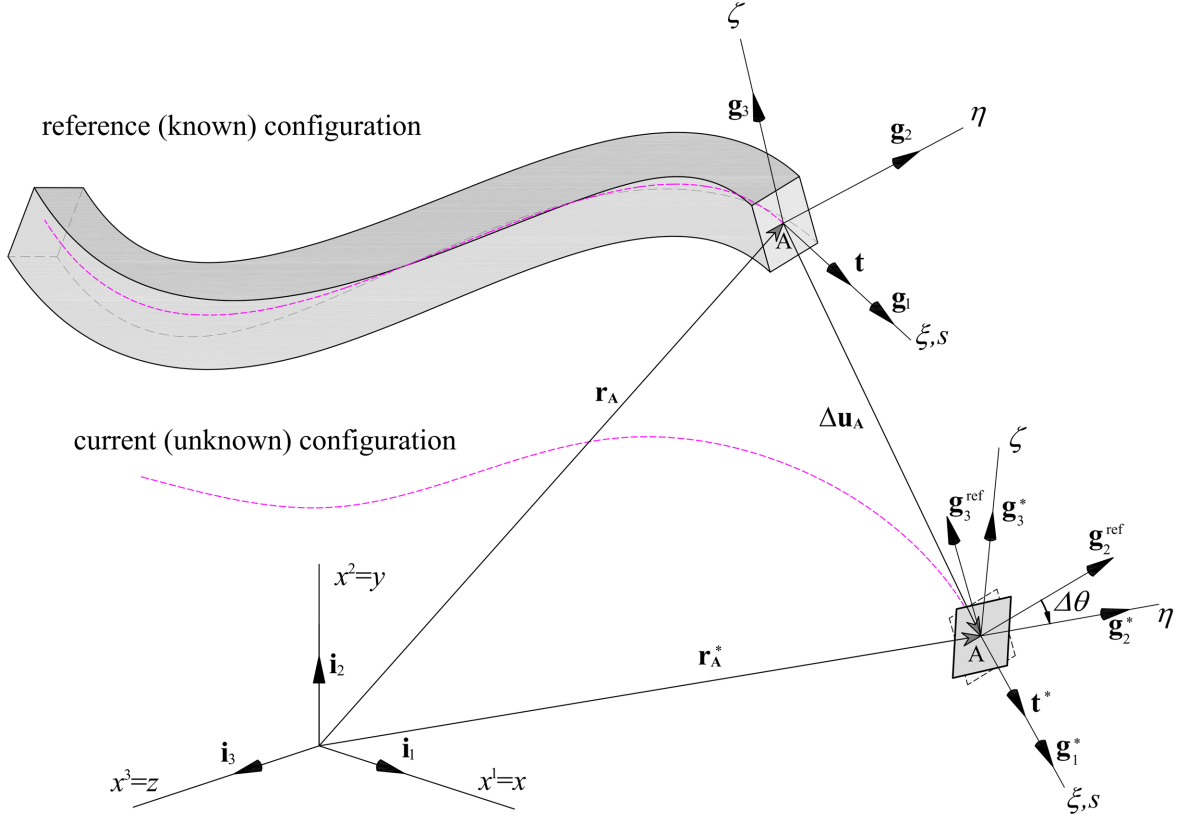


Figure 1: Spatial beam, reference and current configurations.

At this point, let us introduce the well-known Frenet-Serret (FS) triad $(\mathbf{t}, \mathbf{n}, \mathbf{b})$. Although not crucial for the present formulation, the intrinsic relation between the FS frame and the curvature of a line makes it useful for the presentation. The curvature vector of the beam axis is:

$$\mathbf{c} = \frac{d\mathbf{t}}{ds} = \frac{d^2\mathbf{r}}{ds^2} = K\mathbf{n}, \quad (4)$$

where \mathbf{n} is the unit-normal while K is the curvature of axis. The third FS base vector, binormal, is now defined as:

$$\mathbf{b} = \mathbf{t} \times \mathbf{n}, \quad (5)$$

and the well-known FS formulae follow:

$$\begin{bmatrix} \mathbf{t}_{,s} \\ \mathbf{n}_{,s} \\ \mathbf{b}_{,s} \end{bmatrix} = \begin{bmatrix} 0 & K & 0 \\ -K & 0 & \tau \\ 0 & -\tau & 0 \end{bmatrix} \begin{bmatrix} \mathbf{t} \\ \mathbf{n} \\ \mathbf{b} \end{bmatrix} \Leftrightarrow \mathbf{t}_{i,s} = K_i^j \mathbf{t}_j = K_{ij} \mathbf{t}_j, \quad (6)$$

where $\mathbf{t}_i = (\mathbf{t}, \mathbf{n}, \mathbf{b})$. Since the curvature tensor with respect to the arc-length parameter is skew-symmetric, we can define a pseudovector of curvature:

$$\mathbf{k}_{FS} = K_{FS}^i \mathbf{t}_i, \quad K_{FS}^i = \frac{1}{2} e^{ijl} K_{lj}, \quad \mathbf{k}_{FS} = \tau \mathbf{t} + K \mathbf{b}, \quad (7)$$

where τ is the torsion of the FS frame while e is the permutation symbol. This allows us to rewrite the FS formulae as:

$$\mathbf{t}_{i,s} = \mathbf{k}_{FS} \times \mathbf{t}_i. \quad (8)$$

In order to define the orientation of the cross section, we will introduce two unit base vectors, \mathbf{g}_2 and \mathbf{g}_3 , which are aligned with the principal axes of inertia of the cross section. In this way, $(\mathbf{g}_1, \mathbf{g}_2, \mathbf{g}_3)$ is a right-handed rectangular coordinate system at each point of a curve, see Fig. 1. For curves with well-defined FS frame, we can specify an angle α between \mathbf{t}_β and \mathbf{g}_β vectors, and express the basis vectors as:

$$\begin{bmatrix} \mathbf{g}_2 \\ \mathbf{g}_3 \end{bmatrix} = \begin{bmatrix} \cos \alpha & \sin \alpha \\ -\sin \alpha & \cos \alpha \end{bmatrix} \begin{bmatrix} \mathbf{n} \\ \mathbf{b} \end{bmatrix}. \quad (9)$$

With respect to the parametric coordinate, the metric tensor of a line and its reciprocal counterpart are:

$$g_{ij} = \begin{bmatrix} g_{11} & 0 & 0 \\ 0 & 1 & 0 \\ 0 & 0 & 1 \end{bmatrix} \implies g^{ij} = \begin{bmatrix} g^{11} & 0 & 0 \\ 0 & 1 & 0 \\ 0 & 0 & 1 \end{bmatrix}, \quad \det(g_{ij}) = g_{11} = g, \quad g^{11} = \frac{1}{g_{11}}. \quad (10)$$

The derivatives of the base vectors \mathbf{g}_i with respect to the parametric coordinate are:

$$\mathbf{g}_{i,1} = x_{,i1}^k \mathbf{i}_k = \Gamma_{i1}^k \mathbf{g}_k, \quad (11)$$

where Γ_{i1}^k are the Christoffel symbols of the second kind of a line. Since \mathbf{g}_1 is not of unit-length, the resulting curvature tensor is not skew-symmetric:

$$\begin{bmatrix} \mathbf{g}_{1,1} \\ \mathbf{g}_{2,1} \\ \mathbf{g}_{3,1} \end{bmatrix} = \begin{bmatrix} \Gamma_{11}^1 & \Gamma_{11}^2 & \Gamma_{11}^3 \\ \Gamma_{21}^1 & \Gamma_{21}^2 & \Gamma_{21}^3 \\ \Gamma_{31}^1 & \Gamma_{31}^2 & \Gamma_{31}^3 \end{bmatrix} \begin{bmatrix} \mathbf{g}_1 \\ \mathbf{g}_2 \\ \mathbf{g}_3 \end{bmatrix} = \begin{bmatrix} \Gamma_{11}^1 & \tilde{K}_3 & -\tilde{K}_2 \\ -K_3 & 0 & K_1 \\ K_2 & -K_1 & 0 \end{bmatrix} \begin{bmatrix} \mathbf{g}_1 \\ \mathbf{g}_2 \\ \mathbf{g}_3 \end{bmatrix}. \quad (12)$$

Here, K_i are the components of the curvature vector with respect to the material basis $\mathbf{k} = K^i \mathbf{g}_i = K_i \mathbf{g}^i$. Concretely, K_1 is the torsion of the material frame \mathbf{g}_i , while K_α are components of curvature with respect to the \mathbf{g}_α basis vectors. Furthermore, $\tilde{K}_\alpha = g K_\alpha$ are the same components but measured with respect to the parametric coordinate. The expressions for the components of curvature follow as:

$$K_1 = \mathbf{g}_{2,1} \cdot \mathbf{g}_3, \quad \tilde{K}_2 = -\mathbf{g}_{1,1} \cdot \mathbf{g}_3, \quad \tilde{K}_3 = \mathbf{g}_{1,1} \cdot \mathbf{g}_2. \quad (13)$$

It is now straightforward to find the relation between the components of the curvature vector with respect to the both coordinate systems [45]:

$$\begin{aligned} K^1 &= \frac{1}{\sqrt{g}} \tau + \frac{1}{g} \alpha_{,1} \implies K_1 = g_{11} K^1, \\ K^2 &= K_2 = K \sin \alpha, \quad K^3 = K_3 = K \cos \alpha. \end{aligned} \quad (14)$$

Finally, we can rewrite Eq. (8) as:

$$\left(\frac{\mathbf{g}_i}{\|\mathbf{g}_i\|} \right)_{,1} = \sqrt{g} \left(\mathbf{k} \times \frac{\mathbf{g}_i}{\|\mathbf{g}_i\|} \right). \quad (15)$$

2.2 Metric of a generic point in beam continuum

In order to completely define the geometry of a beam, we must define a coordinate system at each point of a beam continuum. Since the essence of structural theories is to reduce

the problem, in this case from 3D to 1D, the complete metric of a beam should be defined by a set of reference quantities. It is common to use the metric of beam axis as the reference. For this, let us define an *equidistant line* which is a set of points for which $(\eta, \zeta) = \text{const}$. Its position and tangent base vectors are:

$$\begin{aligned}\mathbf{r}(\xi, \eta, \zeta) &= \bar{\mathbf{r}}(\xi) = \mathbf{r} + \eta \mathbf{g}_2 + \zeta \mathbf{g}_3, \\ \mathbf{g}_1(\xi, \eta, \zeta) &= \bar{\mathbf{g}}_1 = \bar{\mathbf{r}}_{,1} = \mathbf{g}_1 + \eta \mathbf{g}_{2,1} + \zeta \mathbf{g}_{3,1}.\end{aligned}\tag{16}$$

By introducing the so-called *initial curvature correction term* $g_0 = 1 - \eta K_3 + \zeta K_2$, the base vectors of an equidistant line are [20]:

$$\bar{\mathbf{g}}_1 = g_0 \mathbf{g}_1 - \zeta K_1 \mathbf{g}_2 + \eta K_1 \mathbf{g}_3, \quad \bar{\mathbf{g}}_2 = \mathbf{g}_2, \quad \bar{\mathbf{g}}_3 = \mathbf{g}_3.\tag{17}$$

Evidently, these basis vectors are not orthogonal at a generic point, which complicates further reduction from 3D to 1D. In order to overcome this difficulty, a novel coordinate $\xi_\lambda = \xi_\lambda(\xi, \eta, \zeta)$ is utilized in [45]. It is a line orthogonal to the cross section at each point of a beam. By using the coordinate system $(\xi_\lambda, \eta, \zeta)$, axial and torsional actions are decoupled. The tangent base vector of a ξ_λ line is set to be equal to the tangent base vector of the beam axis $\bar{\mathbf{g}}_\lambda = \mathbf{g}_1$. The present derivations are based on this coordinate system.

3 Bernoulli-Euler beam theory

The classical BE assumption states that a cross section is rigid and remains perpendicular to the beam axis in the deformed configuration. This allows us to describe the complete beam kinematics by the translation of beam axis and the angle of twist of cross section.

3.1 Kinematics of beam axis

The metric of the deformed configuration is described in a similar manner to that of the reference one, by defining the triad $(\mathbf{g}_1^*, \mathbf{g}_2^*, \mathbf{g}_3^*)$ in the current configuration. This triad must be found by the update of some reference configuration, and this process is not uniquely defined. Regarding the tangent base vector, its definition is straightforward. The position and tangent base vectors of the beam axis in current configuration are:

$$\begin{aligned}\mathbf{r}^* &= \mathbf{r}^*(\xi) = \mathbf{r} + \mathbf{u}, \\ \mathbf{g}_1^* &= \mathbf{g}_1^*(\xi) = \mathbf{r}_{,1}^* = \mathbf{g}_1 + \mathbf{u}_{,1},\end{aligned}\tag{18}$$

where \mathbf{u} is the displacement vector of the beam axis.

The other two basis vectors must be found by the rotation from some reference configuration:

$$\mathbf{g}_\alpha^* = \mathbf{R} \mathbf{g}_\alpha, \quad \alpha = 2, 3,\tag{19}$$

where \mathbf{R} is the rotation tensor or rotator. In general, this tensor belongs to the special orthogonal group $\text{SO}(3)$ and several parameterization of it exists [54, 10]. Since the $\text{SO}(3)$ group is nonlinear, it is convenient to switch to some linear space.

Let us focus on the velocity field of the beam, since it is tangent to the displacement field. The velocity gradients along the η and ζ directions are:

$$\mathbf{v}_{,\alpha} = \dot{\mathbf{g}}_\alpha^* = \dot{\mathbf{R}} \mathbf{g}_\alpha + \mathbf{R} \dot{\mathbf{g}}_\alpha = \dot{\mathbf{R}} \mathbf{g}_\alpha,\tag{20}$$

while the velocity gradient along the ξ coordinate follows as $\mathbf{v}_{,1} = \dot{\mathbf{g}}_1^* = \dot{\mathbf{u}}_{,1}$. For each member of the SO(3) group, there exists an appropriate spinor $\dot{\Phi}$ which belongs to the so(3) group of skew-symmetric tensors [20]. This spinor represents the infinitesimal rotation and allows the exponential parameterization of the rotator:

$$\mathbf{R} = e^{\Phi} \implies \dot{\mathbf{R}} = \dot{\Phi} \mathbf{R}. \quad (21)$$

In this way, the velocity gradients (20) become:

$$\mathbf{v}_{,\alpha} = \dot{\Phi} \mathbf{g}_{\alpha}^*. \quad (22)$$

The material derivative of the spinor $\dot{\Phi}$ is the antisymmetric part of the velocity gradient - the angular velocity. Its components define the pseudovector $\boldsymbol{\omega}$ with respect to the local triad, [4]:

$$\dot{\Phi}_{ij} = \begin{bmatrix} 0 & -\omega^3 & \omega^2 \\ \omega^3 & 0 & -\omega^1 \\ -\omega^2 & \omega^1 & 0 \end{bmatrix}, \quad \boldsymbol{\omega} = \omega^i \mathbf{g}_i^*, \quad (23)$$

where:

$$\omega^i = \frac{1}{2} \epsilon^{ijk} \hat{v}_{k|j} \implies \omega^1 = \frac{1}{\sqrt{g^*}} \hat{v}_{3|2}, \quad \omega^2 = -\frac{1}{\sqrt{g^*}} \hat{v}_{3|1}, \quad \omega^3 = \frac{1}{\sqrt{g^*}} \hat{v}_{2|1}. \quad (24)$$

Here, ϵ is the Levi-Civita symbol while \hat{v}_k are the components of velocity with respect to the local triad. It is evident from the last equation that two components of angular velocity, ω^2 and ω^3 , depend on the velocity field of beam axis:

$$\begin{aligned} \omega^2 &= -\frac{1}{\sqrt{g^*}} \hat{v}_{3|1} = -\frac{1}{\sqrt{g^*}} \mathbf{g}_3^* \cdot \mathbf{v}_{,1}, \\ \omega^3 &= \frac{1}{\sqrt{g^*}} \hat{v}_{2|1} = \frac{1}{\sqrt{g^*}} \mathbf{g}_2^* \cdot \mathbf{v}_{,1}. \end{aligned} \quad (25)$$

This observation confirms that a rotation of a cross section of a BE beam belongs to the SO(2) group of in-plane rotations [25]. The 2D rotation occurs in the normal plane of the deformed beam axis which is uniquely defined with \mathbf{g}_1^* . Therefore, the only independent component of the angular velocity for the BE beam is the one with respect to the tangent of the beam axis:

$$\omega^1 = \frac{1}{\sqrt{g^*}} \hat{v}_{3|2} = \frac{1}{\sqrt{g^*}} \omega. \quad (26)$$

Besides the components of the velocity of the beam axis, this component of angular velocity represents the fourth DOF of the BE beam model. We will designate its physical counterpart simply with ω . This quantity represents the angular velocity of a cross section with respect to the tangent of the beam axis. It is discussed in [45, 55] that this quantity can be decomposed into two parts, one part being the angular velocity of the FS frame. Since this approach is not applicable for general spatial curves, we will consider ω as the complete twist of the cross section over the increment of time.

For the sake of further derivations, let us find the gradients of velocity with respect to the principal axes of inertia as functions of the generalized coordinates. By using Eqs. (22) and (25) we obtain:

$$\begin{aligned} \mathbf{v}_{,2} &= \dot{\Phi} \mathbf{g}_2^* = \boldsymbol{\omega} \times \mathbf{g}_2^* = -\frac{1}{g^*} \hat{v}_{2|1} \mathbf{g}_1^* + \hat{v}_{3|2} \mathbf{g}_3^* = -\frac{1}{g^*} (\mathbf{g}_2^* \cdot \mathbf{v}_{,1}) \mathbf{g}_1^* + \omega \mathbf{g}_3^*, \\ \mathbf{v}_{,3} &= \dot{\Phi} \mathbf{g}_3^* = \boldsymbol{\omega} \times \mathbf{g}_3^* = -\frac{1}{g^*} \hat{v}_{3|1} \mathbf{g}_1^* - \hat{v}_{3|2} \mathbf{g}_2^* = -\frac{1}{g^*} (\mathbf{g}_3^* \cdot \mathbf{v}_{,1}) \mathbf{g}_1^* - \omega \mathbf{g}_2^*. \end{aligned} \quad (27)$$

The gradients $\mathbf{v}_{,21}$ and $\mathbf{v}_{,31}$ are also required:

$$\begin{aligned}
\mathbf{v}_{,21} &= \left[-\frac{1}{g^*} (\mathbf{g}_2^* \cdot \mathbf{v}_{,1}) \mathbf{g}_1^* + \mathbf{g}_3^* \omega \right]_{,1} \\
&= -\frac{1}{g^*} \left\{ \left(\Gamma_{11}^{*1} \mathbf{g}_1^* + \tilde{K}_3^* \mathbf{g}_2^* - \tilde{K}_2^* \mathbf{g}_3^* \right) (\mathbf{g}_2^* \cdot \mathbf{v}_{,1}) + [(K_1^* \mathbf{g}_3^* - K_3^* \mathbf{g}_1^*) \cdot \mathbf{v}_{,1}] \mathbf{g}_1^* \right. \\
&\quad \left. + (\mathbf{g}_2^* \cdot \mathbf{v}_{,11}) \mathbf{g}_1^* - 2 \Gamma_{11}^{*1} (\mathbf{g}_2^* \cdot \mathbf{v}_{,1}) \mathbf{g}_1^* \right\} + (K_2^* \mathbf{g}_1^* - K_1^* \mathbf{g}_2^*) \omega + \mathbf{g}_3^* \omega_{,1}, \\
\mathbf{v}_{,31} &= \left[-\frac{1}{g^*} (\mathbf{g}_3^* \cdot \mathbf{v}_{,1}) \mathbf{g}_1^* - \mathbf{g}_2^* \omega \right]_{,1} \\
&= -\frac{1}{g^*} \left\{ \left(\Gamma_{11}^{*1} \mathbf{g}_1^* + \tilde{K}_3^* \mathbf{g}_2^* - \tilde{K}_2^* \mathbf{g}_3^* \right) (\mathbf{g}_3^* \cdot \mathbf{v}_{,1}) + [(K_2^* \mathbf{g}_1^* - K_1^* \mathbf{g}_2^*) \cdot \mathbf{v}_{,1}] \mathbf{g}_1^* \right. \\
&\quad \left. + (\mathbf{g}_3^* \cdot \mathbf{v}_{,11}) \mathbf{g}_1^* - 2 \Gamma_{11}^{*1} (\mathbf{g}_3^* \cdot \mathbf{v}_{,1}) \mathbf{g}_1^* \right\} + (K_3^* \mathbf{g}_1^* - K_1^* \mathbf{g}_3^*) \omega - \mathbf{g}_2^* \omega_{,1}.
\end{aligned} \tag{28}$$

3.2 Basis update

As discussed previously, the tangent base vector of the beam axis, \mathbf{g}_1^* , follows directly from the current position of the beam axis. The other two base vectors, \mathbf{g}_α^* , must be found by the rotation, Eq. (19). Due to the fact that only one rotation is the generalized coordinate of BE beam, the parameterization of this rotation is significantly simplified in comparison with shear-deformable models. Namely, the base vectors \mathbf{g}_α^* lie in the normal plane of the deformed beam axis and they are calculated as an in-plane rotation of some reference vectors \mathbf{g}_α^{ref} . The definition of these reference vectors is not unique. Two procedures for the update of basis vectors are considered here, the Smallest Rotation (SR) and the Nodal Smallest Rotation Smallest Rotation Interpolation (NSRISR).

3.2.1 Smallest Rotation

The SR mapping is commonly used for the modeling of BE beams [42]. The procedure consists of two steps. First, the triad from the previous configuration is rotated in order to align its tangent \mathbf{t} with the tangent of the current configuration \mathbf{t}^* . This is done in such a way that this rotation angle is minimized, and the reference vectors are:

$$\mathbf{g}_\alpha^{ref} = \mathbf{g}_\alpha - \frac{\mathbf{t}^* \cdot \mathbf{g}_\alpha}{1 + \mathbf{t}^* \cdot \mathbf{t}} (\mathbf{t} + \mathbf{t}^*) \tag{29}$$

In the second step, this reference frame is rotated in its plane by the angle $\Delta\theta = \omega\Delta t$, where Δt is the current time increment. As a result, the base vectors of the current configuration are found:

$$\begin{bmatrix} \mathbf{g}_2^* \\ \mathbf{g}_3^* \end{bmatrix} = \begin{bmatrix} \cos \Delta\theta & \sin \Delta\theta \\ -\sin \Delta\theta & \cos \Delta\theta \end{bmatrix} \begin{bmatrix} \mathbf{g}_2^{ref} \\ \mathbf{g}_3^{ref} \end{bmatrix}. \tag{30}$$

Note that this mapping has a singularity for $\mathbf{t}^* \cdot \mathbf{t} = -1$ which is of no practical interest if the reference configuration is appropriately defined [42].

3.2.2 Nodal Smallest Rotation Smallest Rotation Interpolation

Unfortunately the SR procedure leads to the non-objectivity of the resulting formulation. Therefore, the NSRISR mapping is introduced in [25] in order to overcome the deficiency of the SR mapping. It is based on the considerations originally developed in [12]. Concretely, although the continuum strain measures of the geometrically exact beam theory are objective, their finite element implementations are not. The problem is caused by the interpolation of the rotations between the current and some reference configurations. This approach, in general, includes rigid-body rotations. In order to solve this issue, the authors of [12] suggested a linear interpolation of the relative rotation between the element nodes. Since this relative rotation is free from any rigid-body motion, the objectivity of the discretized strain measures is preserved.

The NSRISR algorithm consists of three steps. First, the SR procedure is applied to the \mathbf{g}_α vectors at the start and the end of the finite element. The resulting vectors are designated as $\mathbf{g}_{\alpha,start}^{SR}$ and $\mathbf{g}_{\alpha,end}^{SR}$. Second, the SR mapping is applied to the vectors $\mathbf{g}_{\alpha,start}^{SR}$ to develop the reference frame $\mathbf{g}_\alpha^{ref}(\xi)$ at each point of the finite element, $\xi \in [\xi_{start}, \xi_{end}]$. In order to update the basis correctly, this reference frame should be rotated by the angle $\Delta\theta + \Delta\theta_c$, where $\Delta\theta_c$ is the correction angle. This angle represents the difference between the reference frame $\mathbf{g}_\alpha^{ref}(\xi)$, and the one which follow from the classic SR procedure described in the previous Subsection. The correction angle $\Delta\theta_c$ is zero at the start of the element, while, at the end of an element, it can be simply calculated as the angle between the frames $\mathbf{g}_{\alpha,end}^{SR}$ and $\mathbf{g}_\alpha^{ref}(\xi_{end})$. Finally, the correction angle is linearly interpolated between known values at the start and the end, which leads to the function $\Delta\theta_c(\xi)$. In this way, the updated basis is calculated:

$$\begin{bmatrix} \mathbf{g}_2^* \\ \mathbf{g}_3^* \end{bmatrix} = \begin{bmatrix} \cos(\Delta\theta + \Delta\theta_c) & \sin(\Delta\theta + \Delta\theta_c) \\ -\sin(\Delta\theta + \Delta\theta_c) & \cos(\Delta\theta + \Delta\theta_c) \end{bmatrix} \begin{bmatrix} \mathbf{g}_2^{ref} \\ \mathbf{g}_3^{ref} \end{bmatrix}. \quad (31)$$

Derivatives of the base vectors \mathbf{g}_α^* with respect to the parametric coordinate ξ can be calculated straightforwardly from the last expression.

3.3 Strain rates

After the metric of the beam continuum is defined, the next step is to introduce a strain measure. Let us assign the convective property to the coordinates (ξ, η, ζ) . For the convective coordinates, the Lagrange strain equals the difference between the current and reference metrics:

$$\epsilon_{ij} = \frac{1}{2} (g_{ij}^* - g_{ij}). \quad (32)$$

At an arbitrary point of beam continuum, this strain is:

$$\bar{\epsilon}_{ij} = \frac{1}{2} (\bar{g}_{ij}^* - \bar{g}_{ij}), \quad (33)$$

while the components of the strain rate are equal to the material derivatives of strain:

$$\bar{d}_{ij} = \dot{\bar{\epsilon}}_{ij} = \frac{1}{2} \dot{\bar{g}}_{ij}^*. \quad (34)$$

Due to the BE hypothesis, the shear strain rates $d_{21}, d_{31}, d_{23}, d_{32}$ vanish.

The strains at a generic point of beam continuum are strictly derived in [45] with respect to the $(\xi_\lambda, \eta, \zeta)$ coordinates. We omit this derivation for the sake of brevity. The resulting strain rates are:

$$\begin{aligned}\bar{d}_{11} &= \frac{1}{g_0^*} [(1 + \eta K_3^* - \zeta K_2^*) d_{11} - \eta \dot{\kappa}_3 + \zeta \dot{\kappa}_2], \\ \bar{d}_{12} &= -\frac{1}{g_0^*} \zeta \dot{\kappa}_1, \quad \bar{d}_{13} = -\frac{1}{g_0^*} \eta \dot{\kappa}_1,\end{aligned}\tag{35}$$

where d_{11} is the axial strain rate of beam axis, $\dot{\kappa}_1$ is the rate of change of torsional curvature, and $\dot{\kappa}_\alpha$ are the rates of changes of bending curvatures with respect to the principal axes of inertia. These four quantities represent *the reference strain rates* of BE beam since they allow the calculation of the complete strain rate field of a beam.

The next step is to derive the relation between the reference strain rates and the generalized coordinates. For the axial strain rate, the derivation is simple:

$$d_{11} = \frac{1}{2} \dot{g}_{11}^* = \mathbf{g}_1^* \cdot \mathbf{v}_{,1},\tag{36}$$

while the curvature components require more attention. By using Eq. (13), we obtain:

$$\begin{aligned}\dot{\kappa}_1 &= \dot{K}_1^* = \mathbf{v}_{,21} \cdot \mathbf{g}_3^* + \mathbf{g}_{2,1}^* \cdot \mathbf{v}_{,3}, \\ \dot{\kappa}_2 &= \dot{K}_2^* = -\mathbf{v}_{,11} \cdot \mathbf{g}_3^* - \mathbf{g}_{1,1}^* \cdot \mathbf{v}_{,3}, \\ \dot{\kappa}_3 &= \dot{K}_3^* = \mathbf{v}_{,11} \cdot \mathbf{g}_2^* + \mathbf{g}_{1,1}^* \cdot \mathbf{v}_{,2},\end{aligned}\tag{37}$$

and after introducing Eqs. (27) and (28) into Eq. (37), the final expressions for the rates of curvature changes are:

$$\begin{aligned}\dot{\kappa}_1 &= K_2^* (\mathbf{g}_2^* \cdot \mathbf{v}_{,1}) + K_3^* (\mathbf{g}_3^* \cdot \mathbf{v}_{,1}) + \omega_{,1}, \\ \dot{\kappa}_2 &= -\mathbf{g}_3^* \cdot (\mathbf{v}_{,11} - \Gamma_{11}^{*1} \mathbf{v}_{,1}) + \tilde{K}_3^* \omega, \\ \dot{\kappa}_3 &= \mathbf{g}_2^* \cdot (\mathbf{v}_{,11} - \Gamma_{11}^{*1} \mathbf{v}_{,1}) - \tilde{K}_2^* \omega.\end{aligned}\tag{38}$$

3.4 Spatial discretization

Using IGA, both geometry and velocity are here discretized with the same univariate NURBS functions R_I . However, different univariate NURBS functions R_J^ω are utilized for the approximation of the angular velocity:

$$\begin{aligned}\mathbf{r} &= \sum_{I=1}^N R_I(\xi) \mathbf{r}_I, \quad \alpha = \sum_{I=1}^N R_I(\xi) \alpha_I, \\ \mathbf{v} &= \sum_{I=1}^N R_I(\xi) \mathbf{v}_I, \quad \omega = \sum_{J=1}^M R_J^\omega(\xi) \omega_J,\end{aligned}\tag{39}$$

where $(\bullet)_I$ stands for the value of quantity at I^{th} control point. If we introduce a vector of generalized coordinates, $\mathbf{v}_\omega^\top = [\mathbf{v}^\top \ \omega]^\top$, and the matrix of basis functions \mathbf{N} , the kinematic field of the beam can be represented as:

$$\mathbf{v}_\omega = \mathbf{N} \dot{\mathbf{q}},\tag{40}$$

where:

$$\begin{aligned}\dot{\mathbf{q}}^T &= [\dot{\mathbf{q}}_1 \quad \dot{\mathbf{q}}_2 \quad \dots \quad \dot{\mathbf{q}}_I \quad \dots \quad \dot{\mathbf{q}}_N \quad \omega_1 \quad \omega_2 \quad \dots \quad \omega_J \quad \dots \quad \omega_M], \quad \dot{\mathbf{q}}_I = [v_I^1 \quad v_I^2 \quad v_I^3] \\ \mathbf{N} &= [\mathbf{N}_1 \quad \mathbf{N}_2 \quad \dots \quad \mathbf{N}_I \quad \dots \quad \mathbf{N}_N \quad \mathbf{N}_1^\omega \quad \mathbf{N}_2^\omega \quad \dots \quad \mathbf{N}_J^\omega \quad \dots \quad \mathbf{N}_M^\omega], \\ \mathbf{N}_I &= \begin{bmatrix} \mathbf{R}_I \\ \mathbf{0}_{1 \times 3} \end{bmatrix}, \quad \mathbf{R}_I = \begin{bmatrix} R_I & 0 & 0 \\ 0 & R_I & 0 \\ 0 & 0 & R_I \end{bmatrix}, \quad \mathbf{N}_J^\omega = \begin{bmatrix} \mathbf{0}_{3 \times 1} \\ R_J^\omega \end{bmatrix}.\end{aligned}\tag{41}$$

It is important that the interpolation of the angular velocity ω must have C^0 interelement continuity in order for the NSRISR formulation to keep its objectivity. This fact is proved in [25] and it will be considered in Section 5 via the numerical analysis. The k -refinement, a distinct feature of IGA, ensures the highest-possible continuity, C^{p-1} , while increasing the degree, p , of the spline space [28]. By careful subsequent knot insertion, interelement continuity can be reduced at required points. Our FEM implementation employs this ability for the different discretization of the velocity and angular velocity fields over the same mesh. This is the reason why, in general, we allow that $N \neq M$, and $R_I \neq R_I^\omega$ in Eq. (39).

4 Finite element formulation

In line with the previous derivation, we will formulate isogeometric spatial BE element using the principle of virtual power.

Let us start from the generalized Hooke law for the linear elastic material, also known as the Saint Venant-Kirchhoff material model:

$$\dot{\sigma}_j^i = 2\mu \bar{d}_j^i + \lambda \delta_j^i \bar{d}_m^m, \tag{42}$$

where μ and λ are Lamé material parameters. By introducing the BE constraints $\dot{\sigma}_2^2 = \dot{\sigma}_3^3 = 0$, the non-zero contravariant components of stress rate with respect to the $(\xi_\lambda, \eta, \zeta)$ coordinates are [45]:

$$\dot{\sigma}^{11} = E \bar{g}^{11} \bar{g}^{11} \bar{d}_{11}, \quad \dot{\sigma}^{12} = \mu \bar{g}^{11} \bar{d}_{12}, \quad \dot{\sigma}^{13} = \mu \bar{g}^{11} \bar{d}_{13}. \tag{43}$$

Here, E is modulus of elasticity and μ corresponds to shear modulus.

4.1 Principle of virtual power

The principle of virtual power represents the weak form of the equilibrium. It states that at any instance of time, the total power of the external, internal and inertial forces is zero for any admissible virtual state of motion. If the inertial effects are neglected and body and surface loads are reduced to the beam axis, this can be written for a spatial BE beam as:

$$\delta P = \int_V \boldsymbol{\sigma}^* : \delta \mathbf{d} \, dV - \int_\xi (\mathbf{p}^* \cdot \delta \mathbf{v} + \mathbf{m}^* \cdot \delta \boldsymbol{\omega}) \sqrt{g} \, d\xi, \tag{44}$$

where $\boldsymbol{\sigma}$ is the Cauchy stress tensor, \mathbf{d} is the strain rate tensor, while \mathbf{p} and \mathbf{m} are the vectors of external distributed line forces and moments, respectively. All these quantities are defined at the current, unknown, configuration. By assuming that the load is deformation-independent, only the stress is linearized:

$$\boldsymbol{\sigma}^* \approx \boldsymbol{\sigma} + \dot{\boldsymbol{\sigma}} \Delta t, \tag{45}$$

where $\dot{\boldsymbol{\sigma}}$ is the stress rate tensor which is calculated as the Lie derivative of current stress. Since the components of the stress rate tensor are equal to the material derivatives of the components of the stress tensor, [56], the linearized form of the virtual power is:

$$\begin{aligned} & \int_V (\dot{\bar{\sigma}}^{11} \delta \bar{d}_{11} + \dot{\bar{\sigma}}^{12} \delta \bar{d}_{12} + \dot{\bar{\sigma}}^{13} \delta \bar{d}_{13}) dV \Delta t \\ & + \int_V (\bar{\sigma}^{11} \delta \bar{d}_{11} + \bar{\sigma}^{12} \delta \bar{d}_{12} + \bar{\sigma}^{13} \delta \bar{d}_{13}) dV = \int_{\xi} (\hat{p}^i \delta \hat{v}_i + \hat{m}^i \delta \omega_i) \sqrt{g} d\xi, \end{aligned} \quad (46)$$

where \hat{p}^i and \hat{m}^i are the components of distributed line forces and moments with respect to local coordinates.

We will simplify the notation for the remainder of this paper, by neglecting the asterisks. We emphasize that this change in notation does not introduce any ambiguity since (i) the stress and strain rates are instantaneous quantities, while the known stress is calculated at the previous configuration, and (ii) all integrations are performed with respect to the metric of the current configuration, in accordance with the updated Lagrangian procedure [57].

By integrating the left-hand side of Eq. (46) with respect to the area of the cross section, the integrals over the 3D volume reduce to line integrals along the beam axis:

$$\begin{aligned} & \int_{\xi} \left(\dot{N} \delta d_{11} + \dot{M}_1 \delta \kappa_1 + \dot{M}_2 \delta \kappa_2 + \dot{M}_3 \delta \kappa_3 \right) \sqrt{g} d\xi \Delta t \\ & + \int_{\xi} \left(\tilde{N} \delta d_{11} + \tilde{M}_1 \delta \kappa_1 + \tilde{M}_2 \delta \kappa_2 + \tilde{M}_3 \delta \kappa_3 \right) \sqrt{g} d\xi, \end{aligned} \quad (47)$$

where \tilde{N} and \tilde{M}_j are stress resultant and stress couples, that are energetically conjugated with the reference strain rates of the beam axis, d_{11} and κ_j . \dot{N} and \dot{M}_j are their respective rates given by:

$$\begin{aligned} \dot{N} &= \int_A (1 + \eta K_3 - \zeta K_2) \dot{\bar{\sigma}}^{11} d\eta d\zeta, \\ \dot{M}_1 &= \int_A (\eta \dot{\bar{\sigma}}^{13} - \zeta \dot{\bar{\sigma}}^{12}) d\eta d\zeta, \\ \dot{M}_2 &= \int_A \zeta \dot{\bar{\sigma}}^{11} d\eta d\zeta, \\ \dot{M}_3 &= - \int_A \eta \dot{\bar{\sigma}}^{11} d\eta d\zeta. \end{aligned} \quad (48)$$

If we introduce the following vectors:

$$\begin{aligned} \mathbf{f}^T &= [\tilde{N} \quad \tilde{M}_1 \quad \tilde{M}_2 \quad \tilde{M}_3], \quad \mathbf{e}^T = [d_{11} \quad \kappa_1 \quad \kappa_2 \quad \kappa_3], \\ \mathbf{p}^T &= [p_1 \quad p_2 \quad p_3], \quad \mathbf{m}^T = [m_1 \quad m_2 \quad m_3], \end{aligned} \quad (49)$$

Eq. (46) can be expressed in compact matrix form as:

$$\int_{\xi} \mathbf{f}^T \delta \mathbf{e} \sqrt{g} d\xi \Delta t + \int_{\xi} \mathbf{f}^T \delta \mathbf{e} \sqrt{g} d\xi = \int_{\xi} (\mathbf{p}^T \delta \mathbf{v} + \mathbf{m}^T \delta \boldsymbol{\omega}) \sqrt{g} d\xi. \quad (50)$$

4.2 The relation between energetically conjugated pairs

The geometrically exact relations (47) and (48) are crucial for the accurate formulation of structural beam theories. In particular, energetically conjugated pairs are defined rigorously and the appropriate constitutive matrix is guaranteed to be symmetric. By the introduction of Eqs. (35) and (43) into Eq. (48), the exact relation between energetically conjugated pairs of stress and strain rates is obtained. The resulting symmetric constitutive matrix \mathbf{D} is derived in [45]:

$$\dot{\mathbf{f}} = \mathbf{D}\mathbf{e}, \quad \mathbf{D} = \frac{E}{g^2} \begin{bmatrix} A & 0 & I_2 & -I_3 \\ 0 & \mu g I_{11}/E & 0 & 0 \\ I_2 & 0 & I_{22} & -I_{23} \\ -I_3 & 0 & -I_{23} & -I_{33} \end{bmatrix}, \quad (51)$$

where the geometric properties of cross section are the functions of curvature:

$$\begin{aligned} A &= \int_A \frac{(1 + \eta K_3 - \zeta K_2)^2}{g_0} d\eta d\zeta, & I_2 &= \int_A \zeta \frac{1 + \eta K_3 - \zeta K_2}{g_0} d\eta d\zeta, \\ I_3 &= \int_A \eta \frac{1 + \eta K_3 - \zeta K_2}{g_0} d\eta d\zeta, & I_{23} &= \int_A \frac{\eta \zeta}{g_0} d\eta d\zeta, \\ I_{22} &= \int_A \frac{\zeta^2}{g_0} d\eta d\zeta, & I_{33} &= \int_A \frac{\eta^2}{g_0} d\eta d\zeta, & I_{11} &= \int_A \frac{\eta^2 + \zeta^2}{g_0} d\eta d\zeta. \end{aligned} \quad (52)$$

If we introduce six integrals:

$$\begin{aligned} H_1 &= \int_A \frac{1}{g_0} d\eta d\zeta, & H_\eta &= \int_A \frac{\eta}{g_0} d\eta d\zeta, & H_{\eta\eta} &= \int_A \frac{\eta^2}{g_0} d\eta d\zeta, \\ H_\zeta &= \int_A \frac{\zeta}{g_0} d\eta d\zeta, & H_{\zeta\zeta} &= \int_A \frac{\zeta^2}{g_0} d\eta d\zeta, & H_{\eta\zeta} &= \int_A \frac{\eta\zeta}{g_0} d\eta d\zeta, \end{aligned} \quad (53)$$

the geometric properties in Eq. (52) can be rewritten as:

$$\begin{aligned} A &= H_1 + 2K_3H_\eta + K_3^2H_{\eta\eta} - 2K_2H_\zeta + K_2^2H_{\zeta\zeta} - 2K_2K_3H_{\eta\zeta}, \\ I_2 &= H_\zeta + K_3H_{\eta\zeta} - K_2H_{\zeta\zeta}, & I_3 &= H_\eta + K_3H_{\eta\eta} - K_2H_{\eta\zeta}, \\ I_{23} &= H_{\eta\zeta}, & I_{22} &= H_{\zeta\zeta}, & I_{33} &= H_{\eta\eta}, & I_{11} &= H_{\zeta\zeta} + H_{\eta\eta}. \end{aligned} \quad (54)$$

It is emphasized that these integrals can be analytically computed for standard symmetric solid cross section shapes. The derived exact constitutive model is designated as D^a further in the paper.

This strict derivation allows us to examine the influence of the exact constitutive relation. Four reduced constitutive models are considered for this purpose. The first and the simplest one is designated with D^0 . This model is based on two assumptions: (i) $g_0 \rightarrow 1$, and (ii) the matrix \mathbf{D} is diagonal:

$$\begin{aligned} A &= \int_A d\eta d\zeta, & I_2 &= I_3 = I_{23} = 0, \\ I_{22} &= \int_A \zeta^2 d\eta d\zeta, & I_{33} &= \int_A \eta^2 d\eta d\zeta, & I_{11} &= \int_A (\eta^2 + \zeta^2) d\eta d\zeta. \end{aligned} \quad (55)$$

Therefore, this model completely disregards the coupling between bending and axial actions [25]. The second reduced model, D^1 , also employs the first assumption of D^0 ,

$g_0 \rightarrow 1$, but it keeps the coupling terms from the matrix \mathbf{D} . This D^1 model is readily utilized for the analysis of beams with small curvature [37, 45]. The involved integrals simplify to:

$$\begin{aligned} H_1 &= \int_A d\eta d\zeta, & H_\eta &= \int_A \eta d\eta d\zeta = 0, & H_{\eta\eta} &= \int_A \eta^2 d\eta d\zeta, \\ H_\zeta &= \int_A \zeta d\eta d\zeta = 0, & H_{\zeta\zeta} &= \int_A \zeta^2 d\eta d\zeta, & H_{\eta\zeta} &= \int_A \eta\zeta d\eta d\zeta = 0. \end{aligned} \quad (56)$$

Let us emphasize that these results are valid only when the integrals are calculated with respect to the principle axes of inertia. Additionally, the higher order terms with respect to the curvature in the property A , Eq. (54), are neglected for this constitutive model, which yields $A = H_1$.

In order to assess the effect of the higher order terms, we introduce two additional reduced models, D^2 and D^3 , which employ a Taylor approximation of the exact expressions (54). To be precise, the model D^2 is based on the 1st order Taylor approximation of integrands which results in:

$$\begin{aligned} H_1 &= \int_A d\eta d\zeta, & H_\eta &= \int_A (K_3\eta^2) d\eta d\zeta, & H_{\eta\eta} &= \int_A \eta^2 d\eta d\zeta, \\ H_\zeta &= \int_A (-K_2\zeta^2\eta^2\zeta^2) d\eta d\zeta, & H_{\zeta\zeta} &= \int_A \zeta^2 d\eta d\zeta, & H_{\eta\zeta} &= \int_A \eta\zeta d\eta d\zeta = 0. \end{aligned} \quad (57)$$

The model D^3 , on the other hand, follows from the 2nd order Taylor approximation of the integrands:

$$\begin{aligned} H_1 &= \int_A (1 + K_3^2\eta^2 + K_2^2\zeta^2 + 6K_2^2K_3^2\eta^2\zeta^2) d\eta d\zeta, \\ H_\eta &= \int_A (K_3\eta^2 + 3K_2^2K_3\eta^2\zeta^2) d\eta d\zeta, \\ H_{\eta\eta} &= \int_A (\eta^2 + K_2^2\eta^2\zeta^2) d\eta d\zeta, \\ H_\zeta &= \int_A (-K_2\zeta^2 - 3K_2K_3^2\eta^2\zeta^2) d\eta d\zeta, \\ H_{\zeta\zeta} &= \int_A (\zeta^2 + K_3^2\eta^2\zeta^2) d\eta d\zeta, \\ H_{\eta\zeta} &= \int_A (-2K_2K_3\eta^2\zeta^2) d\eta d\zeta. \end{aligned} \quad (58)$$

For beams with small curviness and circular cross section, the term I_{11} reduces to the polar moment of area I_0 , Eq. (55). However, for all the other shapes of cross section, this fact does not hold. Instead, the term I_{11} is usually replaced with the so-called *torsional constant*, J , which must be calculated approximately [42]. In the presented research, J is used for the models D^0 and D^1 . For the other three constitutive models, we have scaled the geometric property I_{11} with the ratio J/I_0 , in order to keep the influence of the curviness. However, this aspect did not affect any of our numerical experiments, even for strongly curved beams. Hence, these studies are skipped in the numerical experiments section, for the sake of brevity.

4.3 Discrete equations of motion

Let us turn now to the spatially discretized setting. First, we will define the matrix \mathbf{B}_L which relates the reference strain rates with the generalized coordinates at the control points by using Eqs. (36), (38) and (41):

$$\mathbf{e} = \mathbf{B}_L \dot{\mathbf{q}} = \mathbf{H} \mathbf{B} \dot{\mathbf{q}}, \quad (59)$$

where:

$$\mathbf{B} = [\mathbf{B}_1 \quad \mathbf{B}_2 \quad \dots \quad \mathbf{B}_I \quad \dots \quad \mathbf{B}_N \quad \mathbf{B}_1^\omega \quad \mathbf{B}_2^\omega \quad \dots \quad \mathbf{B}_J^\omega \quad \dots \quad \mathbf{B}_M^\omega],$$

$$\mathbf{B}_I = \begin{bmatrix} \mathbf{R}_{I,1} \\ \mathbf{R}_{I,11} \\ \mathbf{0}_{2 \times 3} \end{bmatrix}, \quad \mathbf{B}_J^\omega = \begin{bmatrix} \mathbf{0}_{6 \times 1} \\ R_J^\omega \\ R_{J,1}^\omega \end{bmatrix}, \quad \mathbf{H} = \begin{bmatrix} \mathbf{g}_1^\top & \mathbf{0}_{1 \times 3} & 0 & 0 \\ K_2 \mathbf{g}_2^\top + K_3 \mathbf{g}_3^\top & \mathbf{0}_{1 \times 3} & 0 & 1 \\ \Gamma_{11}^1 \mathbf{g}_3^\top & -\mathbf{g}_3^\top & \tilde{K}_3 & 0 \\ -\Gamma_{11}^1 \mathbf{g}_2^\top & \mathbf{g}_2^\top & -\tilde{K}_2 & 0 \end{bmatrix}. \quad (60)$$

Since the strain rate is a function of the generalized coordinates as well as the metric, we must vary it with respect to both arguments. By the variation with respect to the generalized coordinates, a linear (material) part of the tangent stiffness is obtained. Variation with respect to the geometry results with the geometric stiffness matrix [56].

Clearly, variation of the reference strain rates in Eqs. (36) and (38) with respect to the generalized coordinates is trivial. On the other hand, variation with respect to the metric is more involved and it is given in detail in Appendix A. Formally, the variation of strain rate can be written as:

$$\delta \mathbf{e} = \delta (\mathbf{B}_L \dot{\mathbf{q}}) = \delta \mathbf{H} \mathbf{B} \dot{\mathbf{q}} + \mathbf{H} \mathbf{B} \delta \dot{\mathbf{q}}. \quad (61)$$

Let us define the matrix of basis functions \mathbf{B}_G , which can be obtained by removing the 8th row from the matrix \mathbf{B} in Eq. (60), and the matrix of generalized section forces \mathbf{G} with elements G_{ij} , cf. Appendix A. Now, by the insertion of Eq. (61) into Eq. (50), we can reformulate the term generated by the known stress and the variation of the strain rate with respect to the metric:

$$\int_\xi \mathbf{f}^\top \delta \mathbf{H} \mathbf{B} \dot{\mathbf{q}} \sqrt{g} d\xi = \dot{\mathbf{q}}^\top \int_\xi \mathbf{B}_G^\top \mathbf{G} \mathbf{B}_G \sqrt{g} d\xi \delta \dot{\mathbf{q}} \Delta t = \dot{\mathbf{q}}^\top \mathbf{K}_G \delta \dot{\mathbf{q}} \Delta t, \quad (62)$$

where \mathbf{K}_G is the geometric stiffness matrix. The complete derivation of this term is given in Appendix A.

Now, the integrands in the equation of the virtual power (50) reduce to:

$$\begin{aligned} \dot{\mathbf{f}}^\top \delta \mathbf{e} &\approx \dot{\mathbf{q}}^\top \mathbf{B}_L^\top \mathbf{D} \mathbf{B}_L \delta \dot{\mathbf{q}}, \\ \mathbf{f}^\top \delta \mathbf{e} &= \mathbf{f}^\top (\delta \mathbf{B}_L \dot{\mathbf{q}} + \mathbf{B}_L \delta \dot{\mathbf{q}}) = \dot{\mathbf{q}}^\top \mathbf{B}_G^\top \mathbf{G} \mathbf{B}_G \delta \dot{\mathbf{q}} \Delta t + \mathbf{f}^\top \mathbf{B}_L \delta \dot{\mathbf{q}}, \end{aligned} \quad (63)$$

where the first term is linearized by neglecting the variation of strain rate with respect to the metric.

Regarding the external virtual power, if we vary it with respect to the kinematics, the vector of the external load, \mathbf{Q} , is recovered:

$$\int_\xi (\mathbf{p}^\top \delta \mathbf{v} + \mathbf{m}^\top \delta \boldsymbol{\omega}) \sqrt{g} d\xi = \mathbf{Q}^\top \delta \dot{\mathbf{q}}, \quad (64)$$

and it is the same as in the linear analysis [45]. However, if we vary the external virtual power with respect to the geometry, a contribution to the geometric stiffness is obtained. The derivation of this term is given in Appendix B. Its implementation in the formulation is important for the successful convergence of the nonlinear solver.

Finally, the discretized and linearized equation of equilibrium is:

$$\dot{\mathbf{q}}^\top \int_{\xi} (\mathbf{B}_L^\top \mathbf{D} \mathbf{B}_L + \mathbf{B}_G^\top \mathbf{G} \mathbf{B}_G) \sqrt{g} d\xi \delta \dot{\mathbf{q}} \Delta t = \mathbf{Q}^\top \delta \dot{\mathbf{q}} - \int_{\xi} \mathbf{f}^\top \mathbf{B}_L \sqrt{g} d\xi \delta \dot{\mathbf{q}}, \quad (65)$$

which can be readily written in the standard form:

$$\mathbf{K}_T \Delta \mathbf{q} = \mathbf{Q} - \mathbf{F}, \quad (\Delta \mathbf{q} = \dot{\mathbf{q}} \Delta t), \quad (66)$$

where:

$$\mathbf{K}_T = \int_{\xi} \mathbf{B}_L^\top \mathbf{D} \mathbf{B}_L \sqrt{g} d\xi + \int_{\xi} \mathbf{B}_G^\top \mathbf{G} \mathbf{B}_G \sqrt{g} d\xi, \quad (67)$$

is the tangent stiffness matrix and:

$$\mathbf{F} = \int_{\xi} \mathbf{B}_L^\top \mathbf{f} \sqrt{g} d\xi, \quad (68)$$

is the vector of internal forces. The vector $\Delta \mathbf{q}$ in Eq. (66) contains increments of displacements and twist at control points with respect to the reference configuration. Due to the approximation introduced with Eq. (63), the solution of Eq. (66) does not satisfy the principle of virtual power and some numerical procedure must be applied. Here, both the Newton-Raphson and arc-length methods are employed.

5 Numerical examples

The aim of the following numerical studies is to validate the presented approach and to examine the influence of the curviness on the structural response. The boundary conditions are imposed in a well-known manner and the rotations are treated with special care since two components are not utilized as DOFs [45]. Components of external moments with respect to the principal axes of inertia are applied as force couples which must be updated at each iteration [52]. Standard Gauss quadrature with $p + 1$ integration points per element are used here.

All the results are presented with respect to the load proportionality factor (LPF), rather than to the load intensity itself. Since the time is a fictitious quantity in the present static analysis, strain and stress rates are equal to strains and stresses, respectively. Besides, increments of displacement and twist are equal to velocity and angular velocity.

Two approaches are considered here in the context of the reference configuration for the basis update, the total and the incremental. For the total approach, the reference configuration is the initial unstressed configuration [58]. For the incremental approach, the previously converged configuration is adopted as the reference one [6]. The total approach should guarantee that the results are path-independent, since no history of deformation is included in the reference configuration.

Furthermore, four element formulations are considered: $SR-C^{p-1}$, $SR-C^0$, $NSRISR-C^{p-1}$, and $NSRISR-C^0$. These formulations vary in the basis update algorithm (SR

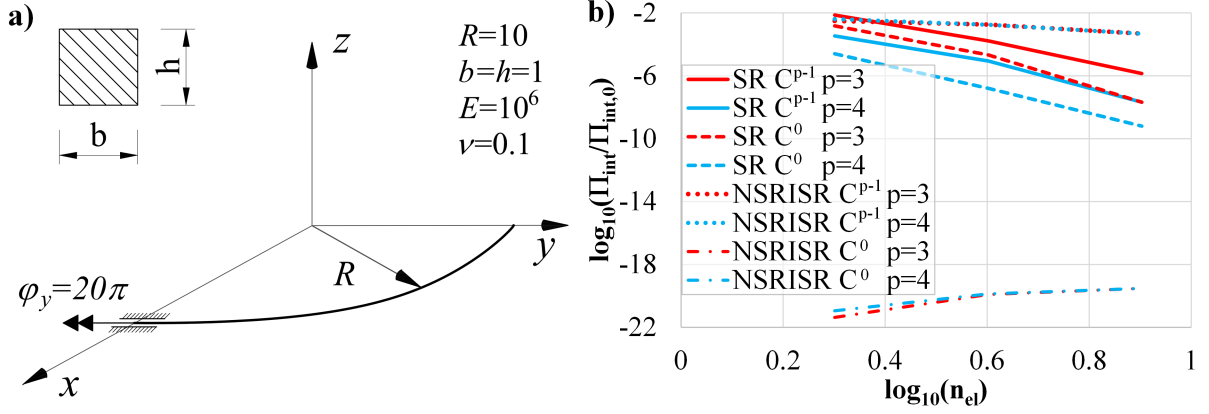


Figure 2: Objectivity. a) Geometry and material properties. b) Ratio of internal strain energy for the different formulations with respect to the number of elements.

or *NSRISR*), and on the interelement continuity used for twist (C^0 or C^{p-1}). For the displacement of the beam axis, the highest available interelement continuity is applied exclusively. If not stated otherwise, the order of the spline functions used for the approximation of the twist is the same as that used for the displacement of the beam axis.

In some examples, the error of the position vector \mathbf{r} is calculated using the relative L^2 -error norm, as proposed in [25]:

$$\|e\|^2 = \frac{1}{u_{max}} \sqrt{\frac{\int_0^L \|\mathbf{r}_h - \mathbf{r}_{ref}\|^2 ds}{L}}, \quad (69)$$

where L is the length of the beam and u_{max} is the maximum value of the displacement component. \mathbf{r}_h represents the approximate solution for the position of the beam axis while \mathbf{r}_{ref} is the appropriate reference solution.

5.1 Objectivity

The objectivity of the formulation can be considered as the invariance with respect to the rigid-body motions. Thus, if the beam is subjected to a rigid-body motion, no strain should appear. Invariance with respect to the translations is readily satisfied while the invariance with respect to the rotation requires special attention [22].

The present example was introduced in [25]. A quarter-circular cantilever beam is rotated ten times around its clamped end with respect to the y -direction, see Fig. 2a. For an objective formulation, there should be no internal strain energy Π_{int} . Due to the extremely large rotations involved in this example, only the incremental update of rotations is considered. The non-homogeneous boundary condition, $\varphi_y = 20\pi$, is applied in 100 increments. Two NURBS orders are considered, $p = 3$ and $p = 4$.

The internal strain energy in the final configuration is plotted in Fig. 2b with respect to the number of elements. The obtained results are scaled with the value $\Pi_{int,0} = EI\pi/(4R)$. This is the internal strain energy of an initially straight beam that is bent into a quarter circle with tip moment [25]. These results confirm that the *NSRISR* - C^0 formulation is indeed objective and the internal strain energy equals zero up to the machine precision. The beam deforms in all the other formulations considered. Furthermore, the results indicate that the problem with the representation of rigid rotations is mitigated for all

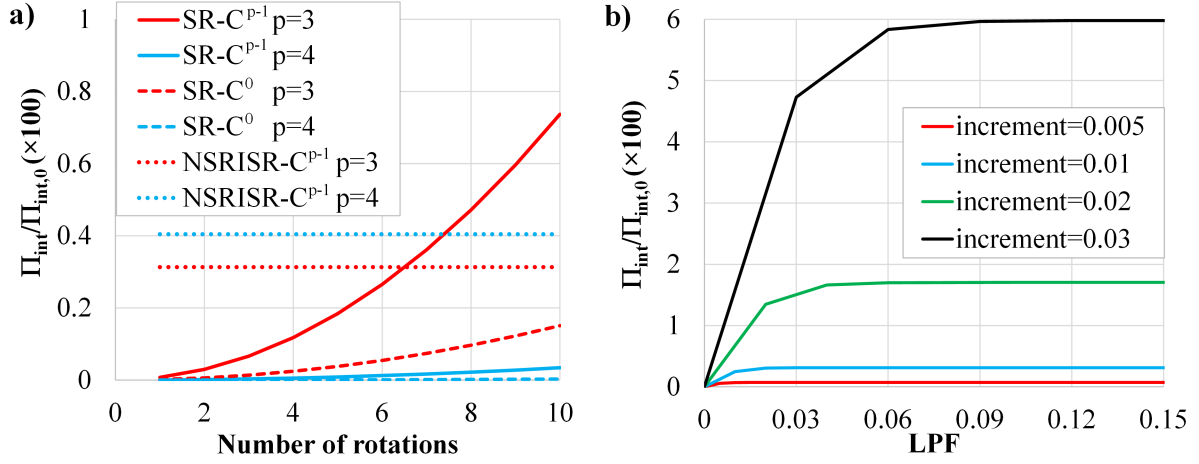


Figure 3: Objectivity. a) Ratio of internal strain energy generated in model for the different formulations with respect to the number of rotation. b) Ratio of internal strain energy for $NSRISR - C^{p-1}$ formulation using two cubic elements for different increment sizes.

formulations when the number of elements is increased. This is a well-known fact, which sometimes justifies the application of non-objective formulations in quasi-static analyses [59].

Fig. 3a shows the evolution of the internal strain energy with the number of rotations for different formulations and NURBS orders. Note that the $SR - C^{p-1}$ formulation with cubic NURBS elements generates around 0.7 % of the reference strain energy, while it is less than 0.2 % for $SR - C^0$ case. A similar behavior can be observed for quartic elements. It follows that the SR formulation greatly benefits from the reduced interelement continuity of the twist variable.

The behavior of the $NSRISR - C^{p-1}$ formulation is also worth mentioning. The results suggest that the initially accumulated internal strain energy, during first few increments, remains constant. In order to examine this more thoroughly, the strain energies for the $NSRISR - C^{p-1}$ formulation and four different increment sizes are plotted in Fig. 3b for $LPF < 0.15$. It is apparent that the error increases with the size of the increment while asymptotically approaching constant value. For this formulation, the beam deforms at the beginning of the loading process and rotates afterwards without the additional straining.

5.2 Path-independence

Path-independence of the solution can be analyzed in various ways. Some authors simply apply different sizes of load increments, [13], while the others change the order of the applied load [25]. Here, we employ the latter approach. A quarter-circle cantilever beam is loaded with two forces at the free end, as shown in Fig. 4. Three cases of the application of load are considered. First, both forces are applied simultaneously - SIM case. For the other two cases, the forces are applied successively, one for $0 < LPF < 0.5$ and the other for $0.5 < LPF < 1$. The case when the \mathbf{F}_X is applied first is designated with $SUCXZ$ while the other case is marked with $SUCZX$.

The deformed beam configurations for all three load order cases and the four characteristic LPF s are shown in Fig. 5. Apparently, all load cases yield similar final configurations

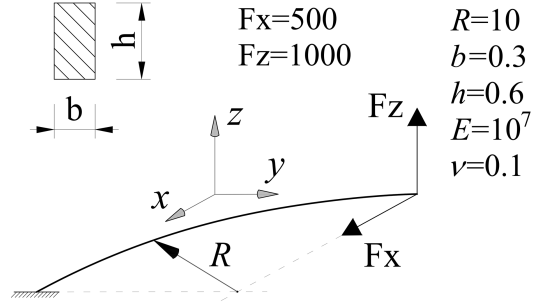


Figure 4: Path-independence. Geometry and load.

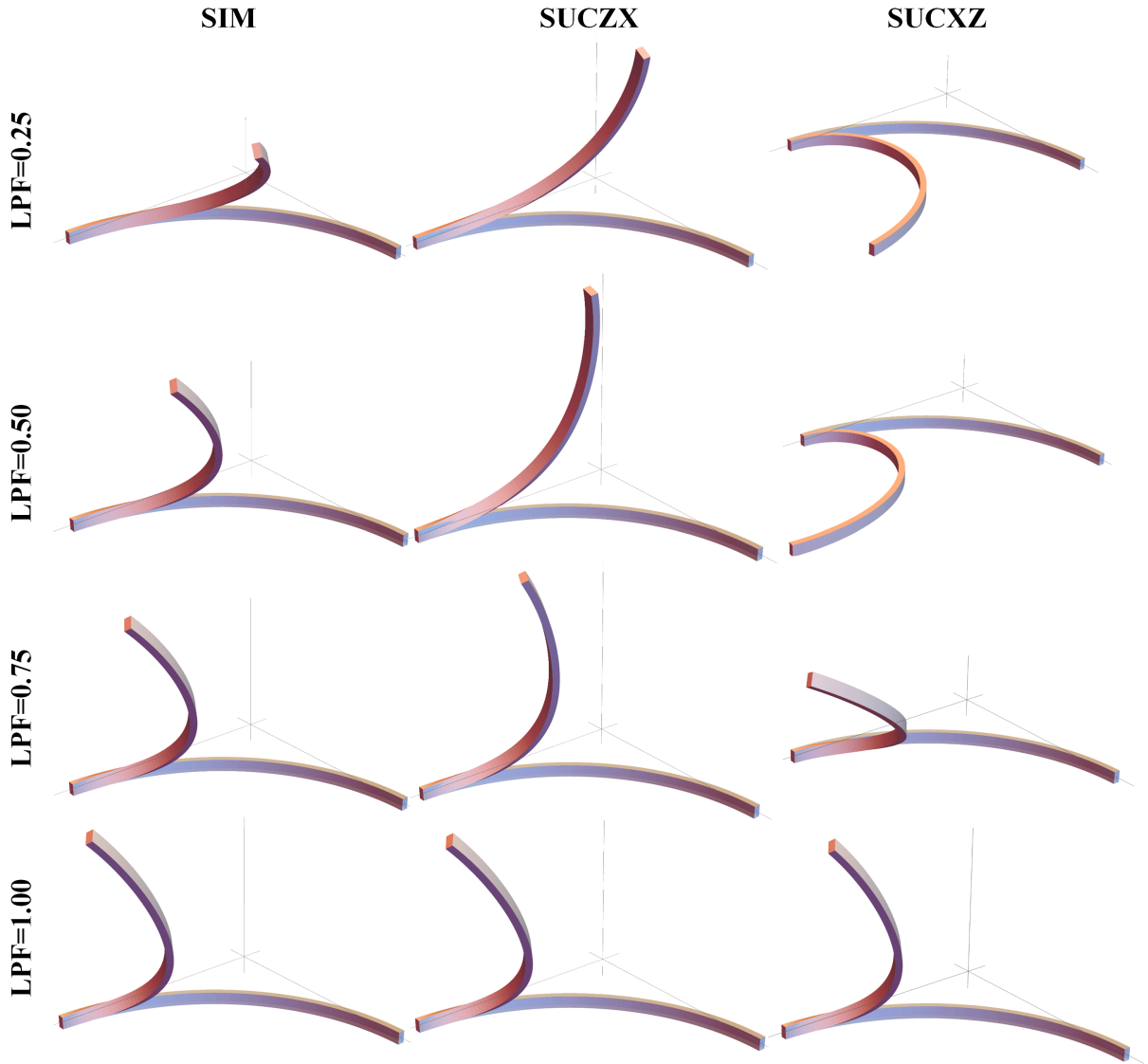


Figure 5: Path-independence. Deformed configurations of the beam for three different loading orders and four values of $LPFs$.

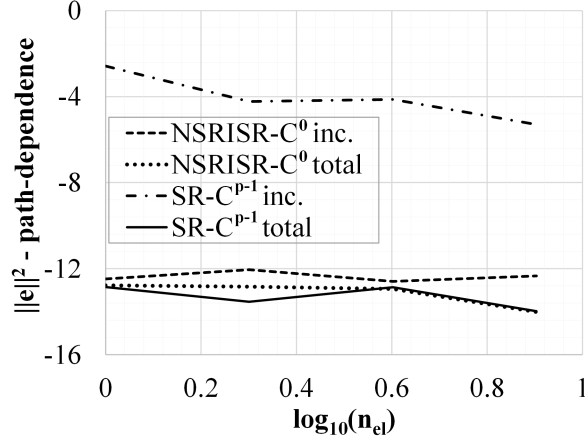


Figure 6: Path-independence. Relative L^2 -difference of the final configurations calculated by the *SUCZX* and the *SIM* load orders with respect to the number of elements. The results are displayed for the $NSRISR - C^0$ and $SR - C^{p-1}$ formulations using the incremental and total algorithms for the basis update.

in visual terms, but each with a different deformation history. Next, the relative L^2 -error norms for the *SIM* and *SUCZX* loading orders are observed for $LPF = 1$ using Eq. (69). Two formulations are considered, $SR - C^{p-1}$ and $NSRISR - C^0$, and two algorithms for the basis update, incremental and total. The results for quartic NURBS are shown in Fig. 6. Our simulations show that of these four combinations, only the $SR - C^{p-1}$ formulation with the incremental update of rotations is path-dependent. As expected, when the unstressed configuration is used as the reference one for the update of the basis, the solution is path-independent [12]. An important fact is the confirmation that the $NSRISR - C^0$ formulation with incremental update of rotations is path-independent [25]. For all the three considered formulations that are path-independent, the relative L^2 -error norms are zero up to the machine precision.

Regarding the $SR - C^{p-1}$ formulation with incremental update of rotations, the relative L^2 -error norm is plotted in Fig. 7a for three NURBS orders. The error due to the path-dependence mitigates with the mesh refinement. In fact, the order by which the path-dependent error reduces should be similar to the order of convergence of the discretization error [25]. To test this, 200 quartic elements and the $NSRISR - C^0$ formulation are used to obtain a reference solution. The convergence of error for three different NURBS orders are displayed in Fig. 7b. For this graph, results from the $NSRISR - C^0$ formulation are used with *SIM* load order. Nevertheless, the discretization errors are practically the same for all the formulations and load orders. The expected orders of convergence, close to $p+1$, are observed and they are similar to those in Fig. 7a. Furthermore, the comparison of the magnitudes of error in Fig. 7a and Fig. 7b confirms the fact that the path-dependent error can be considered negligible with respect to the discretization error [25].

In the following, if not explicitly stated otherwise, the $NSRISR - C^0$ formulation with incremental update of rotations is exclusively used.

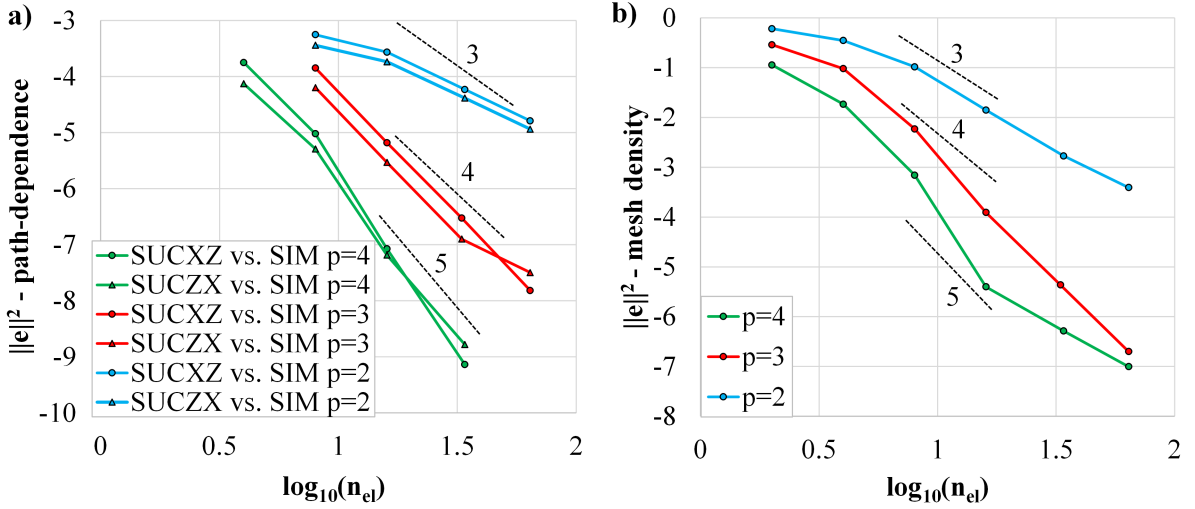


Figure 7: Path-independence. a) Relative L^2 -error norm for $SR - C^{p-1}$ formulation due to the path-dependence. b) Convergence with respect to the mesh density.

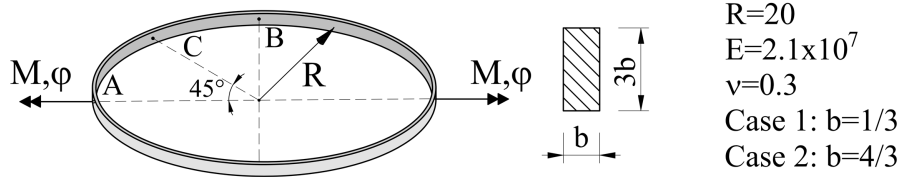


Figure 8: Circular ring subjected to twisting. Load and geometry.

5.3 Circular ring subjected to twisting

This is a well-known example that is frequently considered for the validation of formulations involving finite rotations [25, 19]. A circular ring is subjected to the symmetrical twisting as shown in Fig. 8. Here, the twist is applied as a pair of external concentrated moments $M = EI/R$. Due to the symmetry of the load and the geometry, only a quarter of the ring is modeled [60]. In order to obtain converged strains, a dense mesh of 32 quartic elements is used. Furthermore, two different dimensions of the cross section are considered and designated as Case 1 and Case 2, see Fig. 8. Case 1 corresponds to the examples that are frequently found in the literature. The dependence of LPF and the external angle of twist on one side of the ring is usually observed for the verification. We have adopted the result from [61] as the reference solution. The obtained result is compared with the reference result given in Fig. 9a and excellent agreement can be observed. Furthermore, the curviness at three characteristic points is displayed in Fig. 9b. For Case 1, the maximum curviness is less than 0.07 and all constitutive models return the same results.

In order to examine the influence of different constitutive models on a beam with large curviness, Case 2 is now considered in detail. Although the initial curviness for this beam is $1/15$, it increases to almost 0.22 during the deformation, Fig. 9b, and the beam becomes strongly curved. Furthermore, note that the external twisting of $\varphi = 180^\circ$ deforms the ring into a smaller ring, with a diameter reduced by a factor of three. Additional application of the external twisting returns the ring into its original configuration for $\varphi = 360^\circ$, Fig. 10.

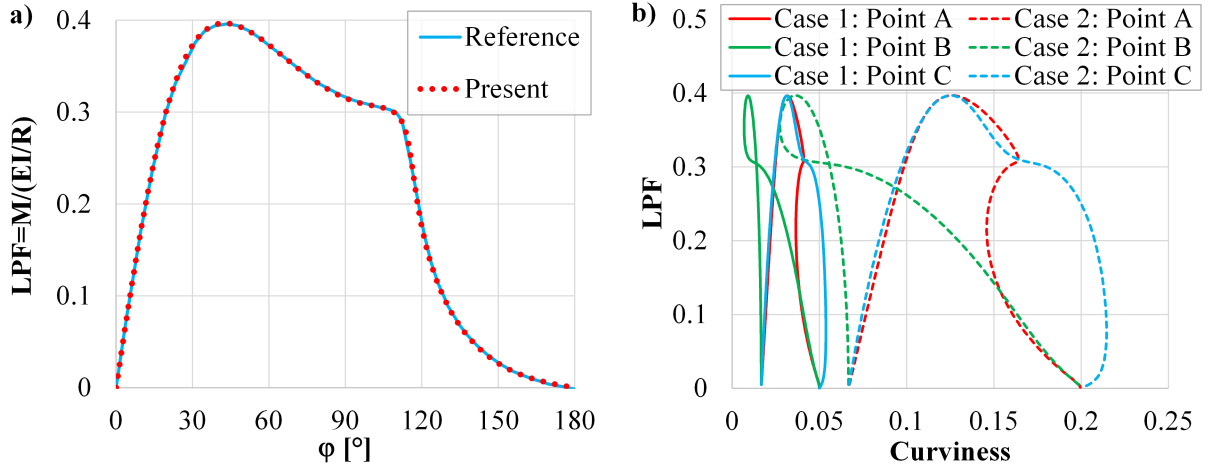


Figure 9: Circular ring subjected to twisting. a) Comparison of LPF vs. external angle of twist. b) Curviness at three points.

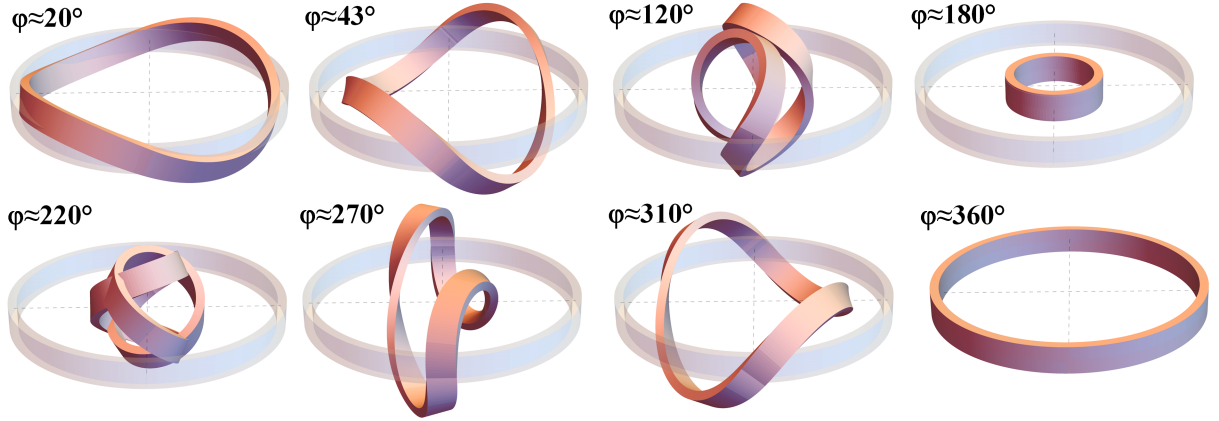


Figure 10: Circular ring subjected to twisting. Deformed configurations for Case 2.

In the following, the complete cycle of external twisting is considered ($\varphi = 360^\circ$) and the reference strains of the beam axis are observed at points A and B, Figs. 11 and 12. The D^0 and D^1 models return erroneous results for the axial strain. For the other three strain components, the results obtained by the different constitutive models are similar, mostly due to the fact that the maximum curviness of this beam is local. However, a close inspection of the equilibrium paths reveals that the differences exist. This detailed insight suggests that the D^3 and D^a models return practically indistinguishable results.

The example is suitable for the testing of the path-independence due to the cyclic response of this ring [19]. For this purpose, the torsional strain at point A is observed, while the ring is twisted eight times ($\varphi = 16\pi$). The results calculated with the $SR - C^0$ and $NSRISR - C^0$ formulations using the incremental update of the basis are given in Fig. 13. This analysis confirms the conclusions from the previous example. The $NSRISR - C^0$ formulation is path-independent while the $SR - C^0$ formulation with incremental update of the basis is not.

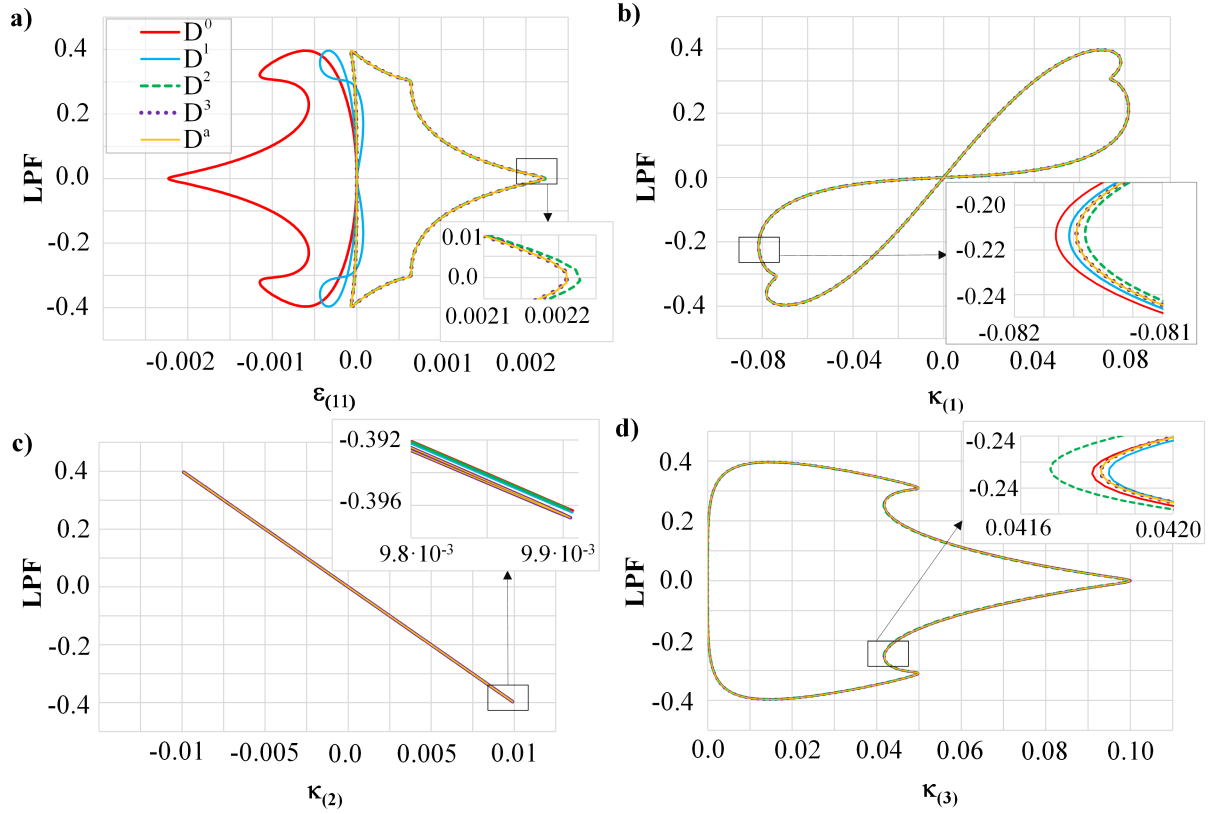


Figure 11: Circular ring subjected to twisting. Reference strains at point A for Case 2.

5.4 Straight beam bent to helix

As a final example, let us consider the response of an initially straight cantilever loaded with two moments as indicated in Fig. 14a. The influence of the polynomial used for the approximation of the twist variable is examined first. The beam is loaded with $M_x = M_z = 10$, while the displacement of the beam axis is discretized with quartic elements. The relative L^2 -error norm of the position of the beam axis at the final configuration is calculated by Eq. (69). The reference solution is obtained from an analytical expression for beams with small curvature, proposed in [26]. Convergence of the D^1 model towards the reference solution is shown in Fig. 14b. We can observe that the polynomial order used for the discretization of the angle of twist does not have significant influence. In fact, all the considered approximative functions return similar results with the exception of quadratic polynomial for the densest mesh. Moreover, the influence of the polynomial order of the twist variable is negligible for all present numerical results.

Next, the beam is discretized with 40 quartic elements and loaded with $M_x = M_z = 20$. The tip displacement along the z -axis is plotted in Fig. 15 for different constitutive models. In order to make close inspection, parts of the equilibrium path for $LPF > 0.2$ are enlarged. As the load increases, the differences between models become visible. This is due to the fact that the maximum curviness for this example is $Kh \approx 0.34$. The D^1 model fully corresponds to the reference analytical solution of the small-curvature beam model. The results obtained by the D^3 and D^a model are practically identical. The error of the D^0 and D^2 models increases with the LPF .

The deformed configurations of the beam in Fig. 16 reveal the complexity of its re-

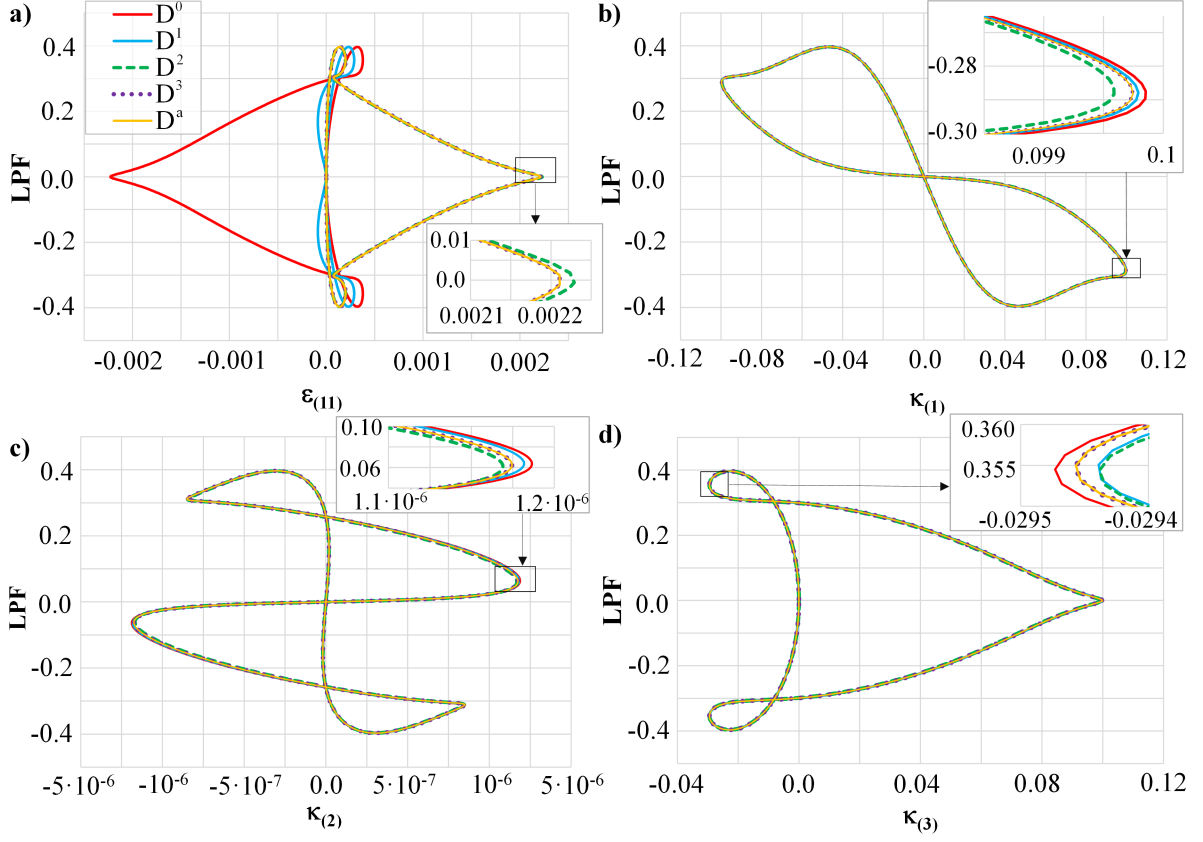


Figure 12: Circular ring subjected to twisting. Reference strains at point B for Case 2.

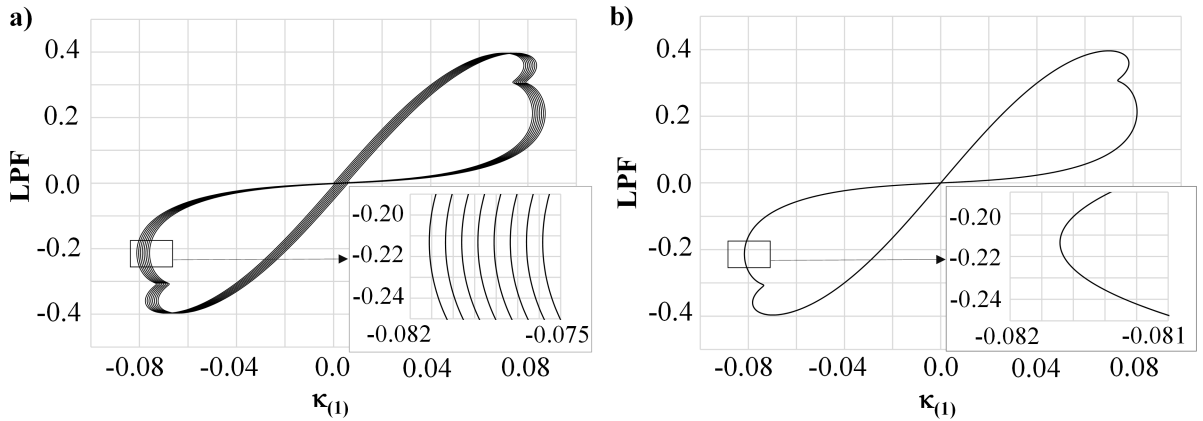


Figure 13: Circular ring subjected to twisting. Comparison of torsional curvature at point A after eight cycles of twisting for two different formulations: a) $SR - C^0$; b) $NSRISR - C^0$.

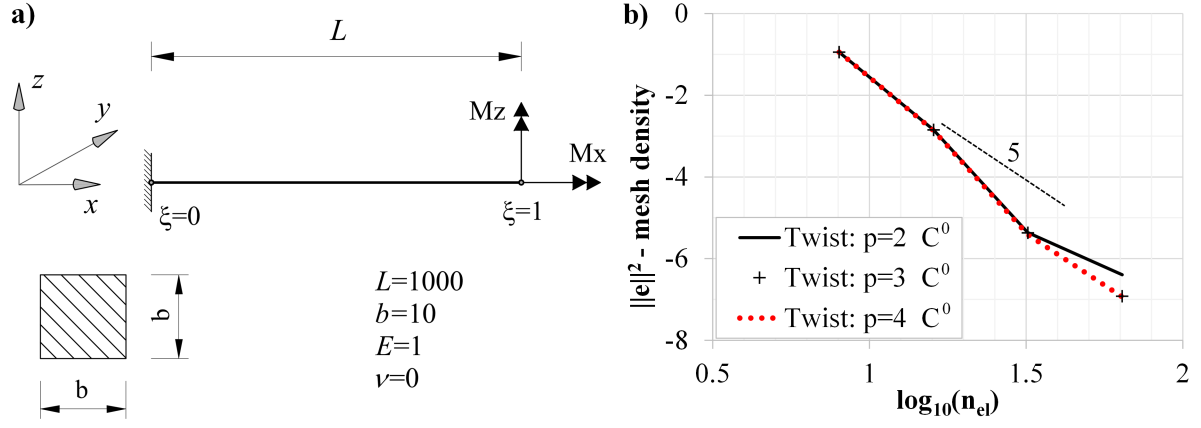


Figure 14: Straight beam bent to helix. a) Geometry and load. b) Convergence of solution with respect to the polynomial degree used for the discretization of the angle of twist.

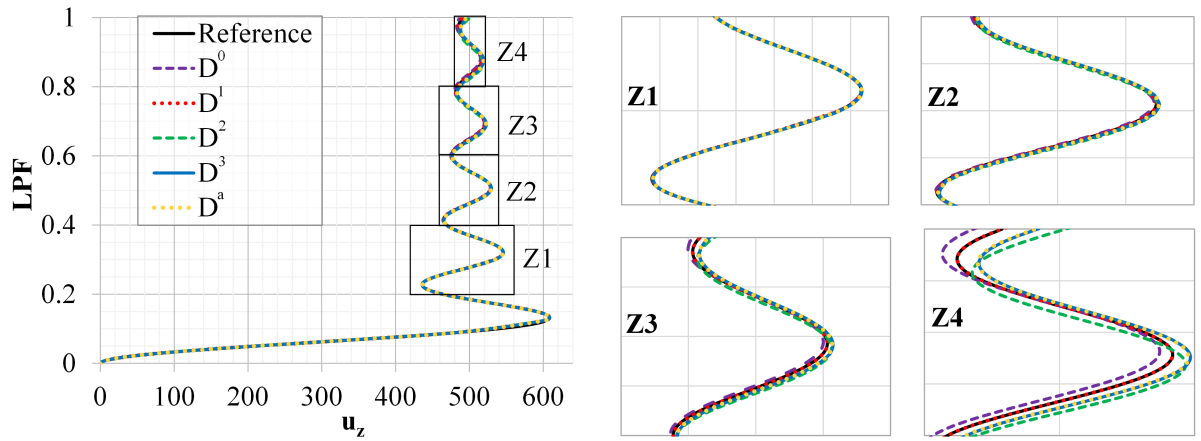


Figure 15: Straight beam bent to helix. Comparison of the tip displacement along the z -axis for different constitutive models. Zoomed parts of the equilibrium paths are shown on the right.

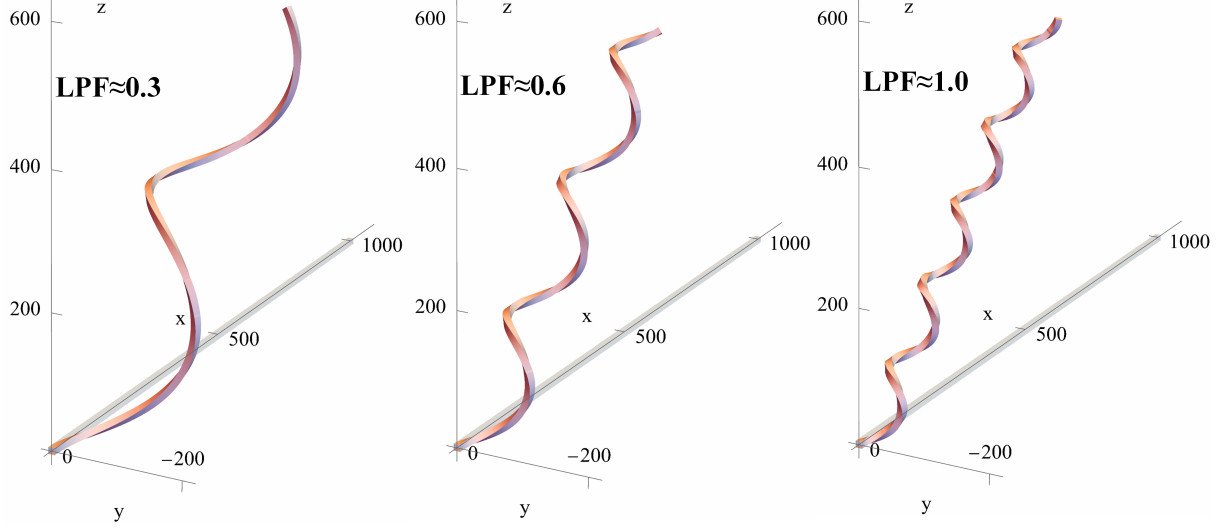


Figure 16: Straight beam bent to helix. Deformed configurations for different values of LPF .

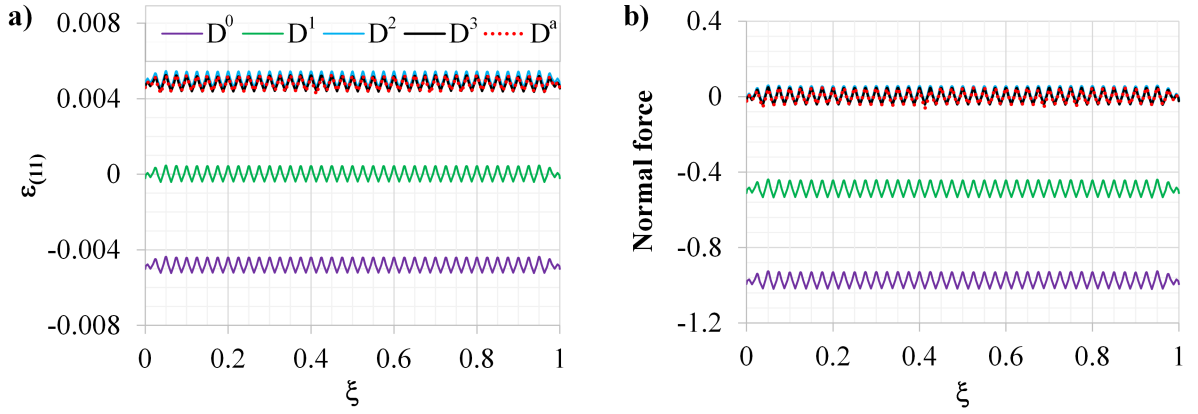


Figure 17: Straight beam bent to helix. a) Distributions of the axial strain of beam axis for different constitutive models. b) Distributions of the normal force for different constitutive models.

sponse. The beam deforms into a helix, and the equilibrium requires that the normal force along the whole beam is zero. If the small-curvature beam model is utilized, the axial strain of the beam axis must also be zero. However, an accurate model, such as the one presented here, results in the dilatation of the beam axis, in a manner similar to that in [52]. The distribution of the axial strain and the normal force at the final configuration are given in Fig. 17 for different constitutive models. The D^0 model returns an erroneous sign of the dilatation of the beam axis and non-zero normal force. On the other hand, the D^1 model results in zero dilatation and non-zero normal force. It should be noted that this model would result in zero normal force if the reduced constitutive matrix is used for the post-processing of the section forces [52]. Here, the full constitutive relation is utilized for the calculation of section forces [45]. Finally, the D^2 , D^3 , and D^a models return similar results, with extensional axial strain and near-zero normal force. Again, the D^3 and D^a models are fully aligned while the D^2 model differs slightly.

Evidently, both the axial strain and the normal force oscillate strongly around the

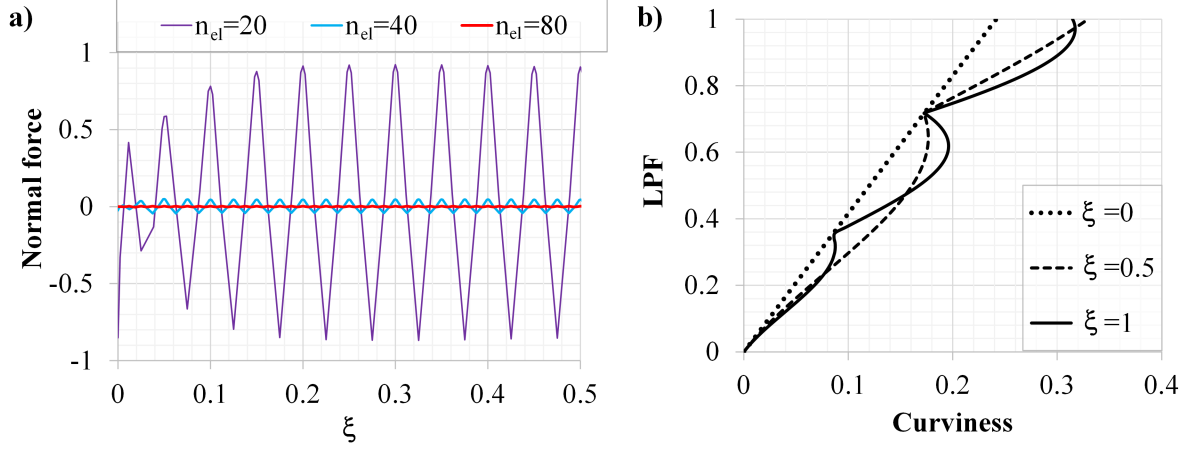


Figure 18: Straight beam bent to helix. a) Distributions of normal force for different numbers of elements. b) Curviness at the start ($\xi = 0$), at the middle ($\xi = 0.5$), and at the end ($\xi = 1$) of the beam vs. LPF.

exact value. To examine this effect, the normal forces for three different mesh densities are given in Fig. 18a. The oscillation of these quantities reduces with the mesh density which can indicate the presence of membrane locking.

The development of the curviness at three characteristics points is shown in Fig. 18b. It is interesting to note that the curviness at the clamped end increases monotonically while it is not the case at the other positions. This is due to the fact that the curviness at the clamped cross section varies solely due to the change in curvature. For the other points, the cross section rotates and the curviness exhibits a more complex behavior.

6 Conclusions

The first truly geometrically exact isogeometric formulation of a spatial Bernoulli-Euler (BE) beam is presented. The rigorous metric of the BE beam is utilized consistently for the derivation of the weak form of equilibrium. The introduction of the full beam metric gave a higher-order accurate BE beam formulation. The exact constitutive relation is employed for the derivation of four simplified models which are compared via numerical examples. Moreover, by the implementation of the Nodal Smallest Rotation Smallest Rotation Interpolation (NSRISR) mapping, an objective and path-independent formulation is obtained.

It is confirmed that the Smallest Rotation (SR) mapping results in a non-objective formulation, the error of which reduces with the mesh density. Additionally, it is shown that both the NSRISR and the SR algorithm benefit from a C^0 interelement continuity of the twist variable.

In order to obtain the correct geometric stiffness matrix, both the internal and the external virtual power are rigorously varied with respect to the unknown metric. The angle of twist requires special attention, since it has one part that depends on the geometry and its variation must be performed consistently.

The presented results suggest that, in order to correctly determine the strains of a strongly curved beam, a higher-order accurate computational model must be employed. For the beams with small curviness the simple decoupled equations return reasonably

accurate results. As the curviness increases, its influence becomes noticeable and a more involved model is required. A simple yet effective solution to improve the accuracy of small-curvature formulations should include the exact nonlinear distribution of strain and stress in the post-processing phase [52].

Future research into the proposed formulation will deal with the dynamics and material non-linear analysis of beams and their interactions with shells.

Acknowledgments

During this work, our beloved colleague and friend, Professor Gligor Radenković (1956-2019), passed away. The first author acknowledges that his unprecedented enthusiasm and love for mechanics were crucial for much of his previous, present, and future research.

We acknowledge the support of the Austrian Science Fund (FWF): M 2806-N.

Appendix A. Geometric stiffness matrix

Since the variations of the base vectors with respect to the metric are:

$$\delta \mathbf{g}_m = \delta \mathbf{v}_{,m} \Delta t, \quad (\text{A1})$$

the variations of the reference strains with respect to the metric are given by:

$$\begin{aligned} \delta d_{11} &= \delta (\mathbf{g}_1 \cdot \mathbf{v}_{,1}) = \delta \mathbf{v}_{,1} \cdot \mathbf{v}_{,1}, \\ \delta \dot{\kappa}_1 &= \delta [K_2 (\mathbf{g}_2 \cdot \mathbf{v}_{,1}) + K_3 (\mathbf{g}_3 \cdot \mathbf{v}_{,1}) + \omega_{,1}] \\ &= \delta K_2 (\mathbf{g}_2 \cdot \mathbf{v}_{,1}) + K_2 (\delta \mathbf{v}_{,2} \cdot \mathbf{v}_{,1}) + \delta K_3 (\mathbf{g}_3 \cdot \mathbf{v}_{,1}) + K_3 (\delta \mathbf{v}_{,3} \cdot \mathbf{v}_{,1}) + \delta \omega_{,1}, \\ \delta \dot{\kappa}_2 &= \delta [-\mathbf{g}_3 \cdot (\mathbf{v}_{,11} - \Gamma_{11}^1 \mathbf{v}_{,1}) + \tilde{K}_3 \omega] \\ &= -\delta \mathbf{v}_{,3} \cdot (\mathbf{v}_{,11} - \Gamma_{11}^1 \mathbf{v}_{,1}) + \delta \Gamma_{11}^1 \mathbf{g}_3 \cdot \mathbf{v}_{,1} + \delta \tilde{K}_3 \omega + \tilde{K}_3 \delta \omega, \\ \delta \dot{\kappa}_3 &= \delta [\mathbf{g}_2 \cdot (\mathbf{v}_{,11} - \Gamma_{11}^1 \mathbf{v}_{,1}) - \tilde{K}_2 \omega] \\ &= \delta \mathbf{v}_{,2} \cdot (\mathbf{v}_{,11} - \Gamma_{11}^1 \mathbf{v}_{,1}) - \delta \Gamma_{11}^1 \mathbf{g}_2 \cdot \mathbf{v}_{,1} - \delta \tilde{K}_2 \omega - \tilde{K}_2 \delta \omega. \end{aligned} \quad (\text{A2})$$

In the following, it is assumed that $\Delta t = 1$, for brevity.

The variations of the gradients of velocities with respect to the kinematics are easily computed from Eq. (27):

$$\begin{aligned} \delta \mathbf{v}_{,2} &= -\frac{1}{g} (\mathbf{g}_2 \cdot \delta \mathbf{v}_{,1}) \mathbf{g}_1 + \mathbf{g}_3 \delta \omega, \\ \delta \mathbf{v}_{,3} &= -\frac{1}{g} (\mathbf{g}_3 \cdot \delta \mathbf{v}_{,1}) \mathbf{g}_1 - \mathbf{g}_2 \delta \omega, \end{aligned} \quad (\text{A3})$$

and from Eq. (28):

$$\begin{aligned}
\delta \mathbf{v}_{,21} &= -\frac{1}{g^*} \left\{ \left(\Gamma_{11}^{*1} \mathbf{g}_1^* + \tilde{K}_3^* \mathbf{g}_2^* - \tilde{K}_2^* \mathbf{g}_3^* \right) (\mathbf{g}_2^* \cdot \delta \mathbf{v}_{,1}) + [(K_1^* \mathbf{g}_3^* - K_3^* \mathbf{g}_1^*) \cdot \delta \mathbf{v}_{,1}] \mathbf{g}_1^* \right. \\
&\quad \left. + (\mathbf{g}_2^* \cdot \delta \mathbf{v}_{,11}) \mathbf{g}_1^* - 2 \Gamma_{11}^{*1} (\mathbf{g}_2^* \cdot \delta \mathbf{v}_{,1}) \mathbf{g}_1^* \right\} + (K_2^* \mathbf{g}_1^* - K_1^* \mathbf{g}_2^*) \delta \omega + \mathbf{g}_3^* \delta \omega_{,1}, \\
\delta \mathbf{v}_{,31} &= -\frac{1}{g^*} \left\{ \left(\Gamma_{11}^{*1} \mathbf{g}_1^* + \tilde{K}_3^* \mathbf{g}_2^* - \tilde{K}_2^* \mathbf{g}_3^* \right) (\mathbf{g}_3^* \cdot \delta \mathbf{v}_{,1}) + [(K_2^* \mathbf{g}_1^* - K_1^* \mathbf{g}_2^*) \cdot \delta \mathbf{v}_{,1}] \mathbf{g}_1^* \right. \\
&\quad \left. + (\mathbf{g}_3^* \cdot \delta \mathbf{v}_{,11}) \mathbf{g}_1^* - 2 \Gamma_{11}^{*1} (\mathbf{g}_3^* \cdot \delta \mathbf{v}_{,1}) \mathbf{g}_1^* \right\} + (K_3^* \mathbf{g}_1^* - K_1^* \mathbf{g}_3^*) \delta \omega - \mathbf{g}_2^* \delta \omega_{,1}.
\end{aligned} \tag{A4}$$

Variations of the curvature components with respect to the metric are:

$$\begin{aligned}
\delta \tilde{K}_2 &= \delta (-\mathbf{g}_{1,1} \cdot \mathbf{g}_3) = -\mathbf{g}_3 \cdot (\delta \mathbf{v}_{,11} - \Gamma_{11}^1 \delta \mathbf{v}_{,1}) + \tilde{K}_3 \delta \omega, \\
\delta \tilde{K}_3 &= \delta (\mathbf{g}_{1,1} \cdot \mathbf{g}_2) = \mathbf{g}_2 \cdot (\delta \mathbf{v}_{,11} - \Gamma_{11}^1 \delta \mathbf{v}_{,1}) - \tilde{K}_2 \delta \omega, \\
\delta K_2 &= \delta \left(\frac{\tilde{K}_2}{g} \right) = \frac{1}{g} \left(\delta \tilde{K}_2 - \frac{2}{g} \tilde{K}_2 \mathbf{g}_1 \cdot \delta \mathbf{v}_{,1} \right), \\
\delta K_3 &= \delta \left(\frac{\tilde{K}_3}{g} \right) = \frac{1}{g} \left(\delta \tilde{K}_3 - \frac{2}{g} \tilde{K}_3 \mathbf{g}_1 \cdot \delta \mathbf{v}_{,1} \right),
\end{aligned} \tag{A5}$$

while the variation of the Christoffel symbol is:

$$\delta \Gamma_{11}^1 = \delta \left(\frac{\mathbf{g}_{1,1} \cdot \mathbf{g}_1}{g} \right) = \frac{1}{g} \left[\mathbf{g}_1 \cdot (\delta \mathbf{v}_{,11} - \Gamma_{11}^1 \delta \mathbf{v}_{,1}) + (\tilde{K}_3 \mathbf{g}_2 - \tilde{K}_2 \mathbf{g}_3) \cdot \delta \mathbf{v}_{,1} \right]. \tag{A6}$$

Although the twist angle is adopted as kinematic quantity, it has one part that is pure geometry. Therefore, we must also vary it with respect to the metric:

$$\delta \omega = \delta (\mathbf{g}_3 \cdot \mathbf{v}_{,2}) = \frac{1}{g} (\mathbf{g}_3 \cdot \delta \mathbf{v}_{,1}) (\mathbf{g}_2 \cdot \mathbf{v}_{,1}) = \frac{1}{g} \mathbf{v}_{,1} \cdot (\mathbf{g}_2 \otimes \mathbf{g}_3) \delta \mathbf{v}_{,1}. \tag{A7}$$

Remark. It is interesting to note that, since the angular velocity can be written as $\omega = \mathbf{g}_3 \cdot \mathbf{v}_{,2}$ or as $\omega = -\mathbf{g}_2 \cdot \mathbf{v}_{,3}$, its variation with respect to the metric can be written in two ways. The first one is given with Eq. (A7) while the other one is:

$$\delta \omega = \delta (-\mathbf{g}_2 \cdot \mathbf{v}_{,3}) = -\frac{1}{g} (\mathbf{g}_2 \cdot \delta \mathbf{v}_{,1}) (\mathbf{g}_3 \cdot \mathbf{v}_{,1}) = -\frac{1}{g} \mathbf{v}_{,1} \cdot (\mathbf{g}_3 \otimes \mathbf{g}_2) \delta \mathbf{v}_{,1}. \tag{A8}$$

Both representation are valid and can be used for the derivation of the geometric stiffness. However, the choice of the representation for $\delta \omega$ must be consistently applied. Its inconsistent use is actually the source of error in the reference [47]. Furthermore, although the both representations of the angular velocity return the same value, their variations in Eqs. (A7) and (A8) are not the same, since the variation is performed with respect to the different parameters.

These expressions are sufficient for the variations of the bending curvatures. For the torsional term, the variation of the gradient of the angular velocity with respect to the metric is required:

$$\delta \omega_{,1} = \delta (\mathbf{g}_3 \cdot \mathbf{v}_{,2})_{,1} = \delta (\mathbf{g}_{3,1} \cdot \mathbf{v}_{,2} + \mathbf{g}_3 \cdot \mathbf{v}_{,21}) = \delta \mathbf{v}_{,31} \cdot \mathbf{v}_{,2} + \delta \mathbf{v}_{,3} \cdot \mathbf{v}_{,21}. \tag{A9}$$

By inserting Eqs. (27), (28), (A3), and (A4) into Eq. (A9), we obtain:

$$\begin{aligned} \delta\omega_{,1} = & \frac{1}{g} \mathbf{v}_{,1} \cdot [-2 \Gamma_{11}^1 (\mathbf{g}_2 \otimes \mathbf{g}_3) + K_1 (\mathbf{g}_3 \otimes \mathbf{g}_3) - K_1 (\mathbf{g}_2 \otimes \mathbf{g}_2) + K_2 (\mathbf{g}_2 \otimes \mathbf{g}_1) \\ & - K_3 (\mathbf{g}_1 \otimes \mathbf{g}_3)] \delta\mathbf{v}_{,1} + \frac{1}{g} \mathbf{v}_{,1} \cdot (\mathbf{g}_2 \otimes \mathbf{g}_3) \delta\mathbf{v}_{,11} + \frac{1}{g} \mathbf{v}_{,11} \cdot (\mathbf{g}_2 \otimes \mathbf{g}_3) \delta\mathbf{v}_{,1}. \end{aligned} \quad (\text{A10})$$

Finally, by the insertion of Eqs. (A3), (A5), (A6), (A7), and (A10) into Eq. (A2), the variations of curvature strain rates with respect to the geometry are:

$$\begin{aligned} \delta\dot{\kappa}_1 = & \frac{1}{g} \mathbf{v}_{,1} \cdot [-\Gamma_{11}^1 (\mathbf{g}_2 \otimes \mathbf{g}_3 + \mathbf{g}_3 \otimes \mathbf{g}_2) + K_1 (\mathbf{g}_3 \otimes \mathbf{g}_3 - \mathbf{g}_2 \otimes \mathbf{g}_2) \\ & - K_2 (\mathbf{g}_2 \otimes \mathbf{g}_1 + \mathbf{g}_1 \otimes \mathbf{g}_2) - 2K_3 (\mathbf{g}_3 \otimes \mathbf{g}_1 + \mathbf{g}_1 \otimes \mathbf{g}_3)] \delta\mathbf{v}_{,1} \\ & + \frac{1}{g} \mathbf{v}_{,1} \cdot (\mathbf{g}_3 \otimes \mathbf{g}_2) \delta\mathbf{v}_{,11} + \frac{1}{g} \mathbf{v}_{,11} \cdot (\mathbf{g}_2 \otimes \mathbf{g}_3) \delta\mathbf{v}_{,1}, \\ \delta\dot{\kappa}_2 = & \frac{1}{g} \mathbf{v}_{,1} \cdot [-\Gamma_{11}^1 (\mathbf{g}_1 \otimes \mathbf{g}_3 + \mathbf{g}_3 \otimes \mathbf{g}_1) - \tilde{K}_2 (\mathbf{g}_3 \otimes \mathbf{g}_3) \\ & + \tilde{K}_3 (\mathbf{g}_2 \otimes \mathbf{g}_3 + \mathbf{g}_3 \otimes \mathbf{g}_2)] \delta\mathbf{v}_{,1} + \frac{1}{g} \mathbf{v}_{,1} \cdot (\mathbf{g}_3 \otimes \mathbf{g}_1) \delta\mathbf{v}_{,11} \\ & + \frac{1}{g} \mathbf{v}_{,11} \cdot (\mathbf{g}_1 \otimes \mathbf{g}_3) \delta\mathbf{v}_{,1} - \mathbf{v}_{,1} \cdot (\Gamma_{11}^1 \mathbf{g}_2) \delta\omega - \omega (\Gamma_{11}^1 \mathbf{g}_2) \cdot \delta\mathbf{v}_{,1} \\ & + \mathbf{v}_{,11} \cdot \mathbf{g}_2 \delta\omega + \omega \mathbf{g}_2 \cdot \delta\mathbf{v}_{,11} - \omega \tilde{K}_2 \delta\omega, \\ \delta\dot{\kappa}_3 = & \frac{1}{g} \mathbf{v}_{,1} \cdot [\Gamma_{11}^1 (\mathbf{g}_1 \otimes \mathbf{g}_2 + \mathbf{g}_2 \otimes \mathbf{g}_1) - \tilde{K}_3 (\mathbf{g}_2 \otimes \mathbf{g}_2)] \delta\mathbf{v}_{,1} \\ & - \frac{1}{g} \mathbf{v}_{,1} \cdot (\mathbf{g}_2 \otimes \mathbf{g}_1) \delta\mathbf{v}_{,11} - \frac{1}{g} \mathbf{v}_{,11} \cdot (\mathbf{g}_1 \otimes \mathbf{g}_2) \delta\mathbf{v}_{,1} \\ & - \mathbf{v}_{,1} \cdot (\Gamma_{11}^1 \mathbf{g}_3) \delta\omega - \omega (\Gamma_{11}^1 \mathbf{g}_3) \cdot \delta\mathbf{v}_{,1} + \mathbf{v}_{,11} \cdot \mathbf{g}_3 \delta\omega + \omega \mathbf{g}_3 \cdot \delta\mathbf{v}_{,11} - \omega \tilde{K}_3 \delta\omega. \end{aligned} \quad (\text{A11})$$

Let us introduce following designations:

$$\begin{aligned}
\mathbf{G}_{11} &= N\mathbf{I}_{3 \times 3} + \frac{M_1}{g} \left[-\Gamma_{11}^1 (\mathbf{g}_2 \otimes \mathbf{g}_3 + \mathbf{g}_3 \otimes \mathbf{g}_2) + K_1 (\mathbf{g}_3 \otimes \mathbf{g}_3 - \mathbf{g}_2 \otimes \mathbf{g}_2) \right. \\
&\quad \left. - K_2 (\mathbf{g}_2 \otimes \mathbf{g}_1 + \mathbf{g}_1 \otimes \mathbf{g}_2) - 2K_3 (\mathbf{g}_3 \otimes \mathbf{g}_1 + \mathbf{g}_1 \otimes \mathbf{g}_3) \right] \\
&\quad + \frac{M_2}{g} \left[-\Gamma_{11}^1 (\mathbf{g}_1 \otimes \mathbf{g}_3 + \mathbf{g}_3 \otimes \mathbf{g}_1) - \tilde{K}_2 (\mathbf{g}_3 \otimes \mathbf{g}_3) \right. \\
&\quad \left. + \tilde{K}_3 (\mathbf{g}_2 \otimes \mathbf{g}_3 + \mathbf{g}_3 \otimes \mathbf{g}_2) \right] \\
&\quad + \frac{M_3}{g} \left[\Gamma_{11}^1 (\mathbf{g}_1 \otimes \mathbf{g}_2 + \mathbf{g}_2 \otimes \mathbf{g}_1) - \tilde{K}_3 (\mathbf{g}_2 \otimes \mathbf{g}_2) \right], \\
\mathbf{G}_{12} &= \frac{M_1}{g} (\mathbf{g}_3 \otimes \mathbf{g}_2) + \frac{M_2}{g} (\mathbf{g}_3 \otimes \mathbf{g}_1) - \frac{M_3}{g} (\mathbf{g}_2 \otimes \mathbf{g}_1), \\
\mathbf{G}_{13} &= -M_2 (\Gamma_{11}^1 \mathbf{g}_2) - M_3 (\Gamma_{11}^1 \mathbf{g}_3), \\
\mathbf{G}_{21} &= \frac{M_1}{g} (\mathbf{g}_2 \otimes \mathbf{g}_3) + \frac{M_2}{g} (\mathbf{g}_1 \otimes \mathbf{g}_3) - \frac{M_3}{g} (\mathbf{g}_1 \otimes \mathbf{g}_2), \\
\mathbf{G}_{22} &= \mathbf{0}_{3 \times 3}, \\
\mathbf{G}_{23} &= M_2 \mathbf{g}_2 + M_3 \mathbf{g}_3, \\
\mathbf{G}_{31} &= -M_2 (\Gamma_{11}^1 \mathbf{g}_2^T) - M_3 (\Gamma_{11}^1 \mathbf{g}_3^T), \\
\mathbf{G}_{32} &= M_2 \mathbf{g}_2^T + M_3 \mathbf{g}_3^T, \\
\mathbf{G}_{33} &= -M_2 \tilde{K}_2 - M_3 \tilde{K}_3,
\end{aligned} \tag{A12}$$

which allows us to define the matrix of generalized section forces:

$$\mathbf{G} = \begin{bmatrix} \mathbf{G}_{11} & \mathbf{G}_{12} & \mathbf{G}_{13} \\ \mathbf{G}_{21} & \mathbf{G}_{22} & \mathbf{G}_{23} \\ \mathbf{G}_{31} & \mathbf{G}_{32} & \mathbf{G}_{33} \end{bmatrix}. \tag{A13}$$

Let us define the matrix of basis functions \mathbf{B}_G :

$$\begin{aligned}
\mathbf{B}_G &= [\mathbf{B}_{G1} \quad \mathbf{B}_{G2} \quad \dots \quad \mathbf{B}_{GI} \quad \dots \quad \mathbf{B}_{GN} \quad \mathbf{B}_{G1}^\omega \quad \mathbf{B}_{G2}^\omega \quad \dots \quad \mathbf{B}_{GJ}^\omega \quad \dots \quad \mathbf{B}_{GM}^\omega], \\
\mathbf{B}_{GI} &= \begin{bmatrix} \mathbf{R}_{I,1} \\ \mathbf{R}_{I,11} \\ \mathbf{0}_{1 \times 3} \end{bmatrix}, \quad \mathbf{B}_{GJ}^\omega = \begin{bmatrix} \mathbf{0}_{6 \times 1} \\ R_J^\omega \end{bmatrix},
\end{aligned} \tag{A14}$$

which is actually the matrix \mathbf{B} without the 8th row, see Eq. (60). The difference between these two matrices of the basis functions is due to the fact that the variation of the torsional curvature change with respect to the kinematics depends on the $\omega_{,1}$, cf. Eqs (38) and (61), while its variation with respect to the metric does not, cf. Eq. (A11). The part of the virtual power generated by the known stress and the variation of the strain rate with respect to the metric can now be expressed as:

$$\int_\xi \mathbf{f}^T \delta \mathbf{H} \mathbf{B} \dot{\mathbf{q}} \sqrt{g} d\xi = \dot{\mathbf{q}}^T \int_\xi \mathbf{B}_G^T \mathbf{G} \mathbf{B}_G \sqrt{g} d\xi \delta \dot{\mathbf{q}} = \dot{\mathbf{q}}^T \mathbf{K}_G \delta \dot{\mathbf{q}}. \tag{A15}$$

Note that the derived geometric stiffness matrix is symmetric. This confirms that the energetically conjugated pairs are correctly adopted. Additionally, the full metric of the BE beam is incorporated in \mathbf{K}_G .

Appendix B. Variation of external virtual power with respect to the metric

Let us consider the contribution to the tangent stiffness that comes from the external load. We will focus on the virtual power due to the concentrated moment, since it was the load used in the numerical analysis. This part of the virtual power is:

$$\delta P_{ext} = -\mathbf{m} \cdot \delta \boldsymbol{\omega}. \quad (\text{B1})$$

If the angular velocities are varied with respect to the kinematics, we obtain the vector of external load. On the other hand, if we vary the angular velocity with respect to the metric, an addition to the stiffness matrix follows. The variation of angular velocity with respect to the geometry is:

$$\delta \boldsymbol{\omega} = \delta (\omega^k \mathbf{g}_k) = \delta \omega^k \mathbf{g}_k + \omega^k \delta \mathbf{v}_k, \quad (\text{B2})$$

where the variations of components of angular velocity are:

$$\begin{aligned} \delta \omega^1 &= \delta \left(\frac{1}{\sqrt{g}} \omega \right) = -\frac{1}{g^{3/2}} (\mathbf{g}_1 \cdot \delta \mathbf{v}_{,1}) \omega + \frac{1}{g^{3/2}} \mathbf{v}_{,1} (\mathbf{g}_2 \otimes \mathbf{g}_3) \delta \mathbf{v}_{,1}, \\ \delta \omega^2 &= \delta \left(-\frac{1}{\sqrt{g}} \mathbf{g}_3 \cdot \mathbf{v}_{,1} \right) = \frac{1}{g^{3/2}} \mathbf{v}_{,1} \cdot (\mathbf{g}_3 \otimes \mathbf{g}_1 + \mathbf{g}_1 \otimes \mathbf{g}_3) \delta \mathbf{v}_{,1} + \frac{1}{\sqrt{g}} \mathbf{g}_2 \cdot \mathbf{v}_{,1} \delta \omega, \\ \delta \omega^3 &= \delta \left(\frac{1}{\sqrt{g}} \mathbf{g}_2 \cdot \mathbf{v}_{,1} \right) = -\frac{1}{g^{3/2}} \mathbf{v}_{,1} \cdot (\mathbf{g}_2 \otimes \mathbf{g}_1 + \mathbf{g}_1 \otimes \mathbf{g}_2) \delta \mathbf{v}_{,1} + \frac{1}{\sqrt{g}} \mathbf{g}_3 \cdot \mathbf{v}_{,1} \delta \omega. \end{aligned} \quad (\text{B3})$$

By the insertion of Eqs. (25), (A3), (A7), (B2), and (B3) into Eq. (B1), we obtain:

$$\begin{aligned} \delta P_{ext} &= \frac{1}{g^{3/2}} \mathbf{v}_{,1} \cdot [(\mathbf{m} \cdot \mathbf{g}_3) (\mathbf{g}_2 \otimes \mathbf{g}_1 + \mathbf{g}_1 \otimes \mathbf{g}_2) - (\mathbf{m} \cdot \mathbf{g}_2) (\mathbf{g}_3 \otimes \mathbf{g}_1 + \mathbf{g}_1 \otimes \mathbf{g}_3) \\ &\quad - (\mathbf{m} \cdot \mathbf{g}_1) (\mathbf{g}_3 \otimes \mathbf{g}_2)] \delta \mathbf{v}_{,1} + \frac{1}{g^{3/2}} \omega (\mathbf{m} \cdot \mathbf{g}_1) (\mathbf{g}_1 \cdot \delta \mathbf{v}_{,1}) - \frac{1}{\sqrt{g}} \omega (\mathbf{m} \cdot \delta \mathbf{v}_{,1}). \end{aligned} \quad (\text{B4})$$

If we define the submatrices:

$$\begin{aligned} \bar{\mathbf{G}}_{11} &= \frac{1}{g^{3/2}} [(\mathbf{m} \cdot \mathbf{g}_3) (\mathbf{g}_2 \otimes \mathbf{g}_1 + \mathbf{g}_1 \otimes \mathbf{g}_2) - (\mathbf{m} \cdot \mathbf{g}_2) (\mathbf{g}_3 \otimes \mathbf{g}_1 + \mathbf{g}_1 \otimes \mathbf{g}_3) \\ &\quad - (\mathbf{m} \cdot \mathbf{g}_1) (\mathbf{g}_3 \otimes \mathbf{g}_2)], \\ \bar{\mathbf{G}}_{12} &= \bar{\mathbf{G}}_{21} = \bar{\mathbf{G}}_{22} = \mathbf{0}_{3 \times 3}, \\ \bar{\mathbf{G}}_{13} &= \bar{\mathbf{G}}_{23} = \mathbf{0}_{3 \times 1}, \\ \bar{\mathbf{G}}_{31} &= \frac{1}{g^{3/2}} (\mathbf{m} \cdot \mathbf{g}_1) \mathbf{g}_1^T - \frac{1}{\sqrt{g}} \mathbf{m}^T, \\ \bar{\mathbf{G}}_{32} &= \mathbf{0}_{1 \times 3}, \\ \bar{\mathbf{G}}_{33} &= 0, \end{aligned} \quad (\text{B5})$$

of the matrix:

$$\bar{\mathbf{G}} = \begin{bmatrix} \bar{\mathbf{G}}_{11} & \bar{\mathbf{G}}_{12} & \bar{\mathbf{G}}_{13} \\ \bar{\mathbf{G}}_{21} & \bar{\mathbf{G}}_{22} & \bar{\mathbf{G}}_{23} \\ \bar{\mathbf{G}}_{31} & \bar{\mathbf{G}}_{32} & \bar{\mathbf{G}}_{33} \end{bmatrix}, \quad (\text{B6})$$

then the matrix $\bar{\mathbf{G}}$ can be simply added to the matrix \mathbf{G} in Eq. (A13).

References

- [1] E. H. Dill, “Kirchhoff’s theory of rods,” *Archive for History of Exact Sciences*, vol. 44, pp. 1–23, Mar. 1992.
- [2] C. Meier, A. Popp, and W. A. Wall, “Geometrically Exact Finite Element Formulations for Slender Beams: Kirchhoff–Love Theory Versus Simo–Reissner Theory,” *Archives of Computational Methods in Engineering*, vol. 26, pp. 163–243, Jan. 2019.
- [3] E. Reissner, “On finite deformations of space-curved beams,” *Zeitschrift für angewandte Mathematik und Physik ZAMP*, vol. 32, pp. 734–744, Nov. 1981.
- [4] J. C. Simo, “A finite strain beam formulation. The three-dimensional dynamic problem. Part I,” *Computer Methods in Applied Mechanics and Engineering*, vol. 49, pp. 55–70, May 1985.
- [5] J. C. Simo and L. Vu-Quoc, “A three-dimensional finite-strain rod model. part II: Computational aspects,” *Computer Methods in Applied Mechanics and Engineering*, vol. 58, pp. 79–116, Oct. 1986.
- [6] A. Cardona and M. Geradin, “A beam finite element non-linear theory with finite rotations,” *International Journal for Numerical Methods in Engineering*, vol. 26, no. 11, pp. 2403–2438, 1988.
- [7] J. C. Simo and L. Vu-Quoc, “On the dynamics in space of rods undergoing large motions — A geometrically exact approach,” *Computer Methods in Applied Mechanics and Engineering*, vol. 66, pp. 125–161, Feb. 1988.
- [8] M. Iura and S. N. Atluri, “On a consistent theory, and variational formulation of finitely stretched and rotated 3-D space-curved beams,” *Computational Mechanics*, vol. 4, pp. 73–88, Mar. 1988.
- [9] A. Ibrahimbegović, “On finite element implementation of geometrically nonlinear Reissner’s beam theory: Three-dimensional curved beam elements,” *Computer Methods in Applied Mechanics and Engineering*, vol. 122, pp. 11–26, Apr. 1995.
- [10] A. Ibrahimbegovic, “On the choice of finite rotation parameters,” *Computer Methods in Applied Mechanics and Engineering*, vol. 149, pp. 49–71, Oct. 1997.
- [11] M. A. Crisfield, *Non-Linear Finite Element Analysis of Solids and Structures, Volume 2, Advanced Topics — Wiley*, vol. 2. Wiley, 1997.
- [12] M. Crisfield and G. Jelenic, “Objectivity of strain measures in the geometrically exact three-dimensional beam theory and its finite-element implementation,” *Proceedings of the Royal Society A: Mathematical, Physical and Engineering Sciences*, vol. 455, no. 1983, pp. 1125–1147, 1999.
- [13] G. Jelenić and M. A. Crisfield, “Geometrically exact 3D beam theory: Implementation of a strain-invariant finite element for statics and dynamics,” *Computer Methods in Applied Mechanics and Engineering*, vol. 171, pp. 141–171, Mar. 1999.

- [14] S. Ghosh and D. Roy, “A frame-invariant scheme for the geometrically exact beam using rotation vector parametrization,” *Computational Mechanics*, vol. 44, p. 103, Jan. 2009.
- [15] I. Romero, “The interpolation of rotations and its application to finite element models of geometrically exact rods,” *Computational Mechanics*, vol. 34, pp. 121–133, July 2004.
- [16] E. Zupan, M. Saje, and D. Zupan, “On a virtual work consistent three-dimensional Reissner–Simo beam formulation using the quaternion algebra,” *Acta Mechanica*, vol. 224, pp. 1709–1729, Aug. 2013.
- [17] K. M. Hsiao, J. Y. Lin, and W. Y. Lin, “A consistent co-rotational finite element formulation for geometrically nonlinear dynamic analysis of 3-D beams,” *Computer Methods in Applied Mechanics and Engineering*, vol. 169, pp. 1–18, Jan. 1999.
- [18] T.-N. Le, J.-M. Battini, and M. Hjiaj, “A consistent 3D corotational beam element for nonlinear dynamic analysis of flexible structures,” *Computer Methods in Applied Mechanics and Engineering*, vol. 269, pp. 538–565, Feb. 2014.
- [19] D. Magisano, L. Leonetti, A. Madeo, and G. Garcea, “A large rotation finite element analysis of 3D beams by incremental rotation vector and exact strain measure with all the desirable features,” *Computer Methods in Applied Mechanics and Engineering*, vol. 361, p. 112811, Apr. 2020.
- [20] R. K. Kapania and J. Li, “On a geometrically exact curved/twisted beam theory under rigid cross-section assumption,” *Computational Mechanics*, vol. 30, pp. 428–443, Apr. 2003.
- [21] F. Armero and J. Valverde, “Invariant Hermitian finite elements for thin Kirchhoff rods. I: The linear plane case,” *Computer Methods in Applied Mechanics and Engineering*, vol. 213–216, pp. 427–457, Mar. 2012.
- [22] F. Armero and J. Valverde, “Invariant Hermitian finite elements for thin Kirchhoff rods. II: The linear three-dimensional case,” *Computer Methods in Applied Mechanics and Engineering*, vol. 213–216, pp. 458–485, Mar. 2012.
- [23] H. Weiss, “Dynamics of Geometrically Nonlinear Rods: I. Mechanical Models and Equations of Motion,” *Nonlinear Dynamics*, vol. 30, pp. 357–381, Dec. 2002.
- [24] F. Boyer, G. De Nayer, A. Leroyer, and M. Visonneau, “Geometrically Exact Kirchhoff Beam Theory: Application to Cable Dynamics,” *Journal of Computational and Nonlinear Dynamics*, vol. 6, Apr. 2011.
- [25] C. Meier, A. Popp, and W. A. Wall, “An objective 3D large deformation finite element formulation for geometrically exact curved Kirchhoff rods,” *Computer Methods in Applied Mechanics and Engineering*, vol. 278, pp. 445–478, Aug. 2014.
- [26] C. Meier, A. Popp, and W. A. Wall, “A locking-free finite element formulation and reduced models for geometrically exact Kirchhoff rods,” *Computer Methods in Applied Mechanics and Engineering*, vol. 290, pp. 314–341, June 2015.

- [27] C. Meier, W. A. Wall, and A. Popp, “A unified approach for beam-to-beam contact,” *Computer Methods in Applied Mechanics and Engineering*, vol. 315, pp. 972–1010, Mar. 2017.
- [28] T. J. R. Hughes, J. A. Cottrell, and Y. Bazilevs, “Isogeometric analysis: CAD, finite elements, NURBS, exact geometry and mesh refinement,” *Computer Methods in Applied Mechanics and Engineering*, vol. 194, pp. 4135–4195, Oct. 2005.
- [29] E. Marino, “Isogeometric collocation for three-dimensional geometrically exact shear-deformable beams,” *Computer Methods in Applied Mechanics and Engineering*, vol. 307, pp. 383–410, Aug. 2016.
- [30] E. Marino, “Locking-free isogeometric collocation formulation for three-dimensional geometrically exact shear-deformable beams with arbitrary initial curvature,” *Computer Methods in Applied Mechanics and Engineering*, vol. 324, pp. 546–572, Sept. 2017.
- [31] O. Weeger, S.-K. Yeung, and M. L. Dunn, “Isogeometric collocation methods for Cosserat rods and rod structures,” *Computer Methods in Applied Mechanics and Engineering*, vol. 316, pp. 100–122, Apr. 2017.
- [32] E. Marino, J. Kiendl, and L. De Lorenzis, “Isogeometric collocation for implicit dynamics of three-dimensional beams undergoing finite motions,” *Computer Methods in Applied Mechanics and Engineering*, vol. 356, pp. 548–570, Nov. 2019.
- [33] D. Vo, P. Nanakorn, and T. Q. Bui, “A total Lagrangian Timoshenko beam formulation for geometrically nonlinear isogeometric analysis of spatial beam structures,” *Acta Mechanica*, vol. 231, pp. 3673–3701, Sept. 2020.
- [34] A. Tasora, S. Benatti, D. Mangoni, and R. Garziera, “A geometrically exact isogeometric beam for large displacements and contacts,” *Computer Methods in Applied Mechanics and Engineering*, vol. 358, p. 112635, Jan. 2020.
- [35] M.-J. Choi, R. A. Sauer, and S. Klinkel, “An isogeometric finite element formulation for geometrically exact Timoshenko beams with extensible directors,” *arXiv:2010.14454 [physics]*, Oct. 2020.
- [36] S. B. Raknes, X. Deng, Y. Bazilevs, D. J. Benson, K. M. Mathisen, and T. Kvamsdal, “Isogeometric rotation-free bending-stabilized cables: Statics, dynamics, bending strips and coupling with shells,” *Computer Methods in Applied Mechanics and Engineering*, vol. 263, pp. 127–143, Aug. 2013.
- [37] L. Greco and M. Cuomo, “B-Spline interpolation of Kirchhoff-Love space rods,” *Computer Methods in Applied Mechanics and Engineering*, vol. 256, pp. 251–269, Apr. 2013.
- [38] L. Greco and M. Cuomo, “An implicit G1 multi patch B-spline interpolation for Kirchhoff-Love space rod,” *Computer Methods in Applied Mechanics and Engineering*, vol. 269, pp. 173–197, Feb. 2014.

- [39] L. Greco and M. Cuomo, “An isogeometric implicit G1 mixed finite element for Kirchhoff space rods,” *Computer Methods in Applied Mechanics and Engineering*, vol. 298, pp. 325–349, Jan. 2016.
- [40] L. Greco and M. Cuomo, “Consistent tangent operator for an exact Kirchhoff rod model,” *Continuum Mechanics and Thermodynamics*, vol. 27, pp. 861–877, Sept. 2015.
- [41] A. M. Bauer, M. Breitenberger, B. Philipp, R. Wüchner, and K. U. Bletzinger, “Non-linear isogeometric spatial Bernoulli beam,” *Computer Methods in Applied Mechanics and Engineering*, vol. 303, pp. 101–127, May 2016.
- [42] D. Vo, P. Nanakorn, and T. Q. Bui, “Geometrically nonlinear multi-patch isogeometric analysis of spatial Euler–Bernoulli beam structures,” *Computer Methods in Applied Mechanics and Engineering*, vol. 380, p. 113808, July 2021.
- [43] Y. B. Yang and Y. Z. Liu, “Invariant isogeometric formulation for the geometric stiffness matrix of spatial curved Kirchhoff rods,” *Computer Methods in Applied Mechanics and Engineering*, vol. 377, p. 113692, Apr. 2021.
- [44] S. Herath and G. Yin, “On the geometrically exact formulations of finite deformable isogeometric beams,” *Computational Mechanics*, Apr. 2021.
- [45] G. Radenković and A. Borković, “Linear static isogeometric analysis of an arbitrarily curved spatial Bernoulli–Euler beam,” *Computer Methods in Applied Mechanics and Engineering*, vol. 341, pp. 360–396, Nov. 2018.
- [46] G. Radenković and A. Borković, “On the analytical approach to the linear analysis of an arbitrarily curved spatial Bernoulli–Euler beam,” *Applied Mathematical Modelling*, vol. 77, pp. 1603–1624, Jan. 2020.
- [47] G. Radenković, *Finite rotation and finite strain isogeometric structural analysis (in Serbian)*. Faculty of Architecture Belgrad, 2017.
- [48] V. Slivker, *Mechanics of Structural Elements: Theory and Applications*. Springer, softcover reprint of hardcover 1st ed. 2007 edition ed., Nov. 2010.
- [49] A. Cazzani, M. Malagù, and E. Turco, “Isogeometric analysis of plane-curved beams,” *Mathematics and Mechanics of Solids*, vol. 21, pp. 562–577, May 2016.
- [50] A. Borković, S. Kovačević, G. Radenković, S. Milovanović, and M. Guzijan-Dilber, “Rotation-free isogeometric analysis of an arbitrarily curved plane Bernoulli–Euler beam,” *Computer Methods in Applied Mechanics and Engineering*, vol. 334, pp. 238–267, June 2018.
- [51] A. Borković, S. Kovačević, G. Radenković, S. Milovanović, and D. Majstorović, “Rotation-free isogeometric dynamic analysis of an arbitrarily curved plane Bernoulli–Euler beam,” *Engineering Structures*, vol. 181, pp. 192–215, Feb. 2019.
- [52] A. Borković, B. Marussig, and G. Radenković, “Geometrically exact static isogeometric analysis of arbitrarily curved plane Bernoulli–Euler beam,” *arXiv:2103.15493 [cs, math]*, Mar. 2021.

- [53] L. Piegl and W. Tiller, *The NURBS Book*. Monographs in Visual Communication, Berlin Heidelberg: Springer-Verlag, 1995.
- [54] M. G  radin and D. Rixen, “Parametrization of finite rotations in computational dynamics: A review,” *Revue Europ  enne des   l  ments Finis*, vol. 4, pp. 497–553, Jan. 1995.
- [55] Y. B. Yang, Y. Liu, and Y. T. Wu, “Invariant isogeometric formulations for three-dimensional Kirchhoff rods,” *Computer Methods in Applied Mechanics and Engineering*, vol. 365, p. 112996, June 2020.
- [56] G. Radenkovi  , A. Borkovi  , and B. Marussig, “Nonlinear static isogeometric analysis of arbitrarily curved Kirchhoff-Love shells,” *International Journal of Mechanical Sciences*, vol. 192, p. 106143, Feb. 2021.
- [57] K. J. Bathe, *Finite Element Procedures*. Boston, Mass.: Klaus-Jurgen Bathe, Feb. 2007.
- [58] M. Ritto-Corr  a and D. Camotim, “On the differentiation of the Rodrigues formula and its significance for the vector-like parameterization of Reissner-Simo beam theory,” *International Journal for Numerical Methods in Engineering*, vol. 55, no. 9, pp. 1005–1032, 2002.
- [59] S. G. Erdelj, G. Jeleni  , and A. Ibrahimbegovi  , “Geometrically non-linear 3D finite-element analysis of micropolar continuum,” *International Journal of Solids and Structures*, vol. 202, pp. 745–764, Oct. 2020.
- [60] G. Yoshiaki, W. Yasuhito, K. Toshihiro, and O. Makoto, “Elastic buckling phenomenon applicable to deployable rings,” *International Journal of Solids and Structures*, vol. 29, pp. 893–909, Jan. 1992.
- [61] P. F. Pai and A. N. Palazotto, “Large-deformation analysis of flexible beams,” *International Journal of Solids and Structures*, vol. 33, pp. 1335–1353, Apr. 1996.